Two studies in statistical data analysis for the space industry: Cyclicality in the industry, and comparative satellite reliability analysis

A Master Thesis
Presented to
The Academic Faculty

By

Thomas Hiriart

In Partial Fulfillment
of the Requirements for the Degree
Master of Science in the
Daniel Guggenheim School of Aerospace Engineering

Georgia Institute of Technology

December 2009

Two studies in statistical data analysis for the space industry:
Cyclicality in the industry, and comparative satellite reliability analysis

Approved by:

Dr. Joseph Saleh, Advisor
Assistant Professor of Aerospace Engineering
Guggenheim School of Aerospace Engineering
Georgia Institute of Technology

Dr. Eric Feron
Dutton/Ducoffe Professor of Aerospace Engineering
Guggenheim School of Aerospace Engineering
Georgia Institute of Technology

Mr. David Spencer
Professor of the Practice
Guggenheim School of Aerospace Engineering
Georgia Institute of Technology

Date approved: 11/10/2009

ACKNOWLEGMENTS

There are a number of people who have helped me throughout the fulfillment of my Master degree. First, I would like to thank my advisor, Dr. Joseph H. Saleh, for his great academic support, for the always useful guidance he provided during my year of study at the Space System Design Laboratory, and for the effort he put forth in making this dissertation possible. Thanks to Dr Saleh's insights, I have definitely learnt a lot within the aerospace industry. I would also like to thank the remaining members of my committee, Dr. Eric Feron, and Mr. David Spencer, for their help and support.

I also thank my friends and fellow students in the Space Systems Design Laboratory. I am grateful for their friendly help and for the time I have enjoyed with them in Atlanta and at the Georgia Institute of Technology.

Finally, I would like to thank my family and friends back in France. I thank my parents for what they have taught me for years, and for having pushed me to achieve academic excellence. I also thank my friends for their continued support and encouragement.

TABLE OF CONTENTS

LIST OF TABLES

LIST OF FIGURES

SUMMARY

This research brings statistical analyses techniques to bear on data derived from an extensive database of satellite launches and on-orbit anomalies and failures. The data collected is analyzed from two different perspectives and addresses, in two separate studies, two research objectives.

The first study proposes to identify trends and cyclical patterns in the space industry, and to forecast the volume of launches for the next few years. Satellites have been rightfully described as the lifeblood of the entire space industry and the number of satellites ordered or launched per year is an important defining metric of the industry's level of activity. The structure of the space industry, its financial health and its workforce retention and development is dependent on the volume of satellites contracted. As such, trends and variability in this volume have significant strategic impact on the space industry. Over the past 40+ years, hundreds of satellites have been launched every year. Thus, an important data set is available for time series analysis and identification of trends and cycles in the various markets of the space industry. For the purpose of this first study, we collected data for over 6,000 satellites launched since 1960 on a yearly basis. We separated the satellites into three broad segments: 1) defense and intelligence satellites, 2) science satellites, and 3) commercial satellites. Several techniques are available for the analysis of time series data, both in the time domain and in the frequency domain. In this first study, we conducted spectral analysis of the time series for each of the three satellite populations and identified cycles contained in the data. In addition, once harmonic models were derived and fitted to the data, we built forecasting models of satellite launch volumes in the different market segments for the next few years. The potential implications of the results are discussed as a number of strategic matters for the space industry are contingent on the predictions or forecast of the volume of satellites contracted (the example of the U.S. auto industry is a solemn reminder of such possible strategic issues).

The second study uses the previously collected launch data, confined to Earth-orbiting satellites launched between 1990 and 2008, and expanded with the failure information and retirement of each satellite to conduct a comparative analysis of satellite reliability in GEO, LEO, and MEO orbits. Reliability has long been recognized as an essential consideration in the design of space systems. However, there is limited statistical analysis of satellite reliability based on actual flight data. The objective of this second study is to conduct nonparametric satellite reliability analysis, with orbit type as a covariate, and to explore appropriate parametric fits (Weibull, lognormal, and mixture

distributions). The results indicate for example that differences exist between the failure behaviors of satellites in different orbits, or that satellite infant mortality exists or dominates more clearly in a particular orbit type. The findings can be useful to satellite manufacturers as they would provide an empirical basis for reviewing and adjusting satellite testing and burn-in procedures.

PART I: Cyclicality Analysis

Chapter 1: Cyclicality in the Space Industry: Times Series Analysis, Periodogram, and Identification of Cyclical Patterns for Modeling and Forecasting

1. Introduction

On October 4, 1957, a small beeping satellite, Sputnik, heralded the beginning of the Space Age. From this humble start, the space industry grew into an impressive $100+ billion industry five decades later. Satellites have been rightfully described as the lifeblood of the entire space industry and the number of satellites ordered or launched per year is an important defining measure of the industry's level of activity. The structure of the space industry, its financial health, and its workforce retention and development is dependent to a large extent on the volume of satellites contracted (not just their costs; a single large expensive satellite has different implications for the space industry than say five smaller cheaper ones). As such, trends and variability in this volume have significant strategic impact on the space industry. Over the past 40+ years, hundreds of satellites have been launched every year. Thus an important data set is available for time series analysis and identification of trends and cycles in the various markets of this industry.

Initially, the term *business cycle* refers to fluctuations in production or economic activity over a defined period of time [1]. In recent years, economic theory has moved towards the study of *economic fluctuation* rather than the traditional understanding of the *business cycle* term [2, 3]. In this study, we seek to identify *cycles* in the broad sense of the term, meaning any cyclical fluctuations observed in satellite launch volume. Our approach is empirical/statistical in nature; causal modeling and explanations are left as fruitful venues for future work. The reader interested in causal explanations of cyclicality in broad terms (e.g., mismatch between production and market demand) is referred to [3–6].

This chapter of the thesis provides and analyzes time series of satellite launches from 1960 to 2008. The objective of this study is to identify and model trends and cyclical patterns in satellite launches, and to use the results for forecasting purposes. The remainder of this research is organized as

follows. In Section 2, we briefly describe the database and the data categorization used in this chapter. In Section 3, we present the actual time series for three broad satellite categories: 1) Defense and Intelligence, 2) Science, and 3) Communication satellites. We then provide a brief qualitative discussion of the data based on visual inspection. In Section 4, we conduct spectral analyses of the data using the Discrete Fourier Transform and identify cycles in each time series. We also derive harmonic models of the time series and we analyze the residuals, or errors between the harmonic models and the actual data and derive normal distribution fits for the errors in each satellite category. In Section 5, we use the harmonic models along with the probabilistic error models to forecast the demand for the next few years (along with 95% confidence intervals) for satellites in each of the three categories. Section 6 concludes this chapter of the thesis. The structure and organization of the present work is visually summarized in Fig. 1.

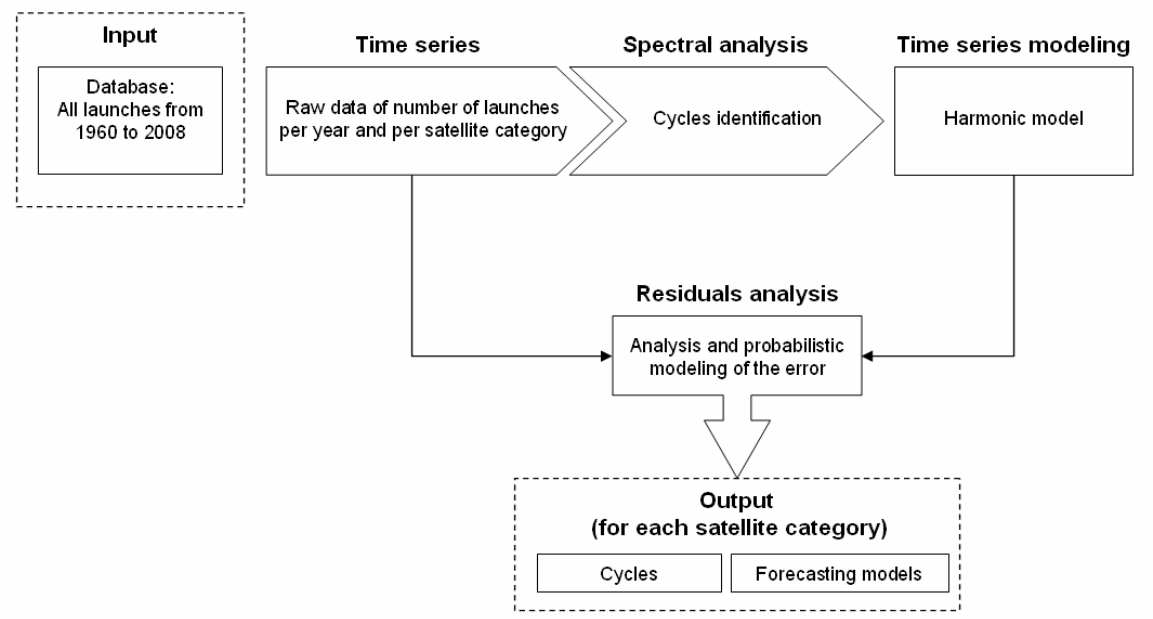

Figure 1: Organization of the present work

2. Database and Data Description

The time series in this study are derived from the SpaceTrak® database [7]. This database is extensively used in the space industry and contains data on satellites launches and on-orbit events such as satellite anomalies, failures, and retirement since 1957. While it cannot be claimed that this

database is “complete” in a statistical sense, it is nevertheless one of the most extensive and authoritative database in the space industry.

For the purpose of this study, we considered the satellite in the database launched between January 1960 and December 2008. In total, 6,556 satellites are listed as having been launched within this time window. Given the purpose of this study, satellites have been included in our dataset regardless of whether their launch was successful or not. For each satellite in our dataset, we collected its launch date and mission sector (additional information was also collected but is not relevant for the purpose of this study). Seventeen mission sectors are identified in the database. We created a different, more compact categorization of satellites for the purpose of this study. The three satellite categories considered hereafter are: 1) Defense and Intelligence (D&I) satellites, 2) Science satellites, and, 3) Communication Satellites. These new categories and their relation to the database categories are shown in Table 1.

Table 1: Satellite categorization

SpaceTrack® satellite categories	**Present work satellite categories**
Early Warning Intelligence Navigation Reconnaissance Weapon System Nuclear Warning	Defense and Intelligence (D&I)
Earth Observation Science	Science
Communication	Communication
Amateur Cargo Experimental Manned Manufacturing Inspection/Repair Test Unknown	Not considered in this work (16.5% of the total)

A total of 5,473 satellites remain in our dataset, approximately 83.5% of all the satellites in the database for the time period of interest. The breakdown of the number of satellites in each category over the entire time period, and per decade, is shown in Fig. 2. From 1960 to 2008, D&I satellites accounted for a major share of satellite launches with 39% of the total considered in this thesis, Communication satellites accounted for 34%, and Science satellites accounted for 27% (Fig. 2). The institutional customers (as opposed to the commercial market) therefore accounted for over two thirds of all satellite launched within our time period (1960–2008). Moreover, in the 60's and the 70's, the institutional customers accounted for 90% and 73.5% respectively of all satellite launches (Fig. 3). It is therefore fair to say that the space industry was enabled by, and grew because of, the institutional customers, not commercial market forces. However, when the launch data is looked at more closely on a decade basis, we see a growing influence of the commercial sector. First we notice in Fig. 3 the substantial influence of the defense market for satellites in the 60's, 70's, and 80's (with the D&I satellites accounting for roughly half of all launches). The launch share of D&I satellites then tumbles down to 24% and 23% in the 90's and 00's respectively. The launch share of Science satellites goes through a contraction between the 60's and the 80's (from 45% to 14% respectively), followed by an expansion in the 80's and 00's (from 14% and 31% respectively). The salient feature in Fig. 3 is the steady growth the launch share of communication satellites per decade starting with a meager 10% in the 60's then growing to account for roughly half of all shares of launches in the 90's and 00's. This observation reflects an important shift in the space industry in which, over the last two decades, communication satellites have assumed the role that the Defense and Intelligence satellites played in the early decades of the space age. The commercial sector is playing an increasingly major role in the space industry, accounting roughly for the same launch share as the institutional market.

In the following section, the launch data on a yearly basis will be provided and looked at more closely.

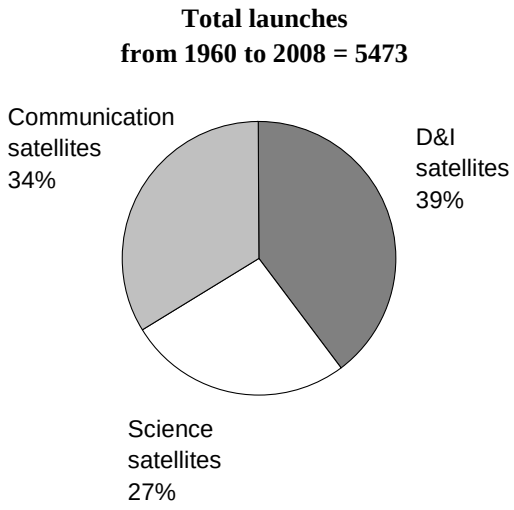

Figure 2: Launch percentages per satellite category from 1960 to 2008

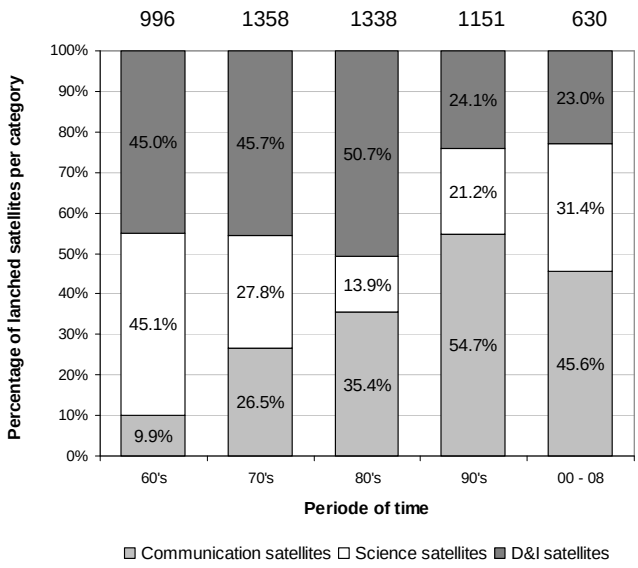

Figure 3: Launch percentages per decade and per satellite category from 1960 to 2008

3. Time Series, Visual Inspection and Qualitative Discussion

In this section, we provide the time series for the three satellite categories, followed by a brief discussion of the data based on visual inspection. The quantitative spectral analysis of each time series follows in Section 4.

3.1. Defense and Intelligence (D&I) satellites

Figure 4 shows the number of D&I satellite launches per year from 1960 to 2008. Important trends are clearly visible in Fig. 4. For example, notice first the dramatic increase in launches per year from 15 D&I satellites in 1960 to 70 such satellites in 1965. Following this steep increase, the number of yearly D&I satellites launched remains high during the cold war, and oscillates between 50 and 80 launches per year from 1965 to 1988. A closer look within this time period shows two peaks, one in 1977 with 78 launches, and another one in 1984 with 80 launches. Next, the number of satellites dramatically drops from 1988 until it plummets to a dangerously low (for the space industry) 8 D&I satellites launched in 1999. Finally, from 1999 to 2008, the number of D&I satellites launched per year has on average slowly drifted upwards (lower-right corner in Fig. 4)

with some notable variations / oscillations of roughly three years period. Detailed quantitative analysis of the data in Fig. 4 will be provided in Section 4.

Figure 4: D&I satellite launches per year from 1960 to 2008

3.2. Science satellites

Figure 5 shows the number of Science satellite launches per year from 1960 to 2008. As with the D&I satellites, we notice first a dramatic increase in launches per year from 13 Science satellites in 1960 to 68 such satellites in 1965. However, the launch of Science satellites tumbles down earlier than the drop in D&I satellites, by the early to mid 1970s for the former instead of the late 1980s for the latter. As can be seen in Fig. 5, the number of Science satellites drops to its lowest point in 1980 with 9 satellites launched. Finally, it can be seen that by the mid 1990s, the number of Science satellites launched per year exhibits clear oscillations between 15 and 30–35 yearly launches (lower-right corner of Fig. 5), but no clear trend or drift can be identified. It is worth pointing out that the time series of Science satellites appears "more choppy" (higher variability) than that of D&I satellites.

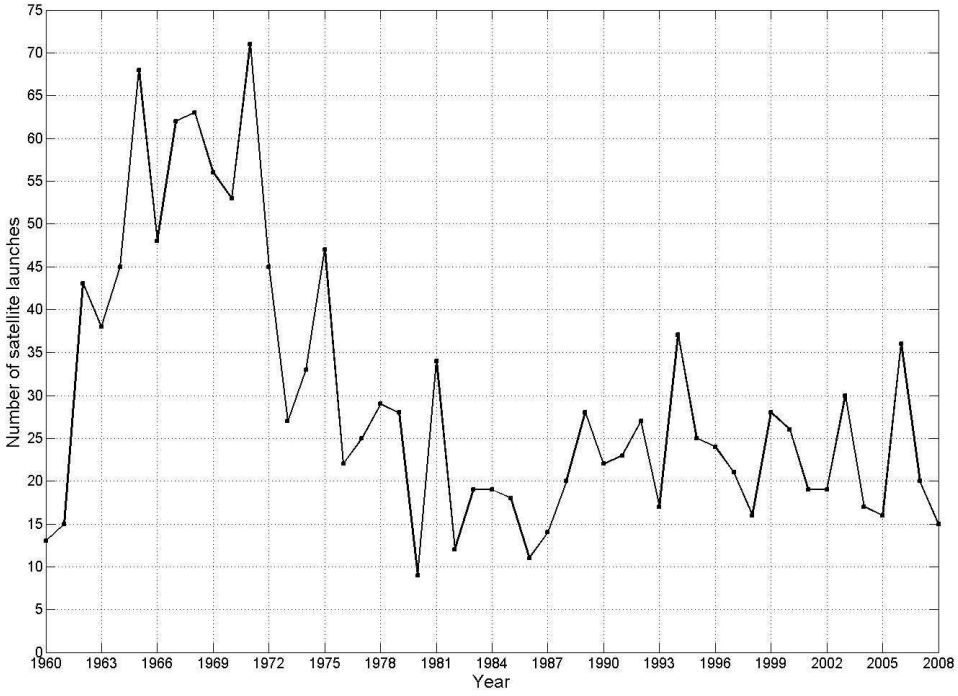

Figure 5: Science satellite launches per year from 1960 to 2008

3.3. Communication satellites

Figure 6 shows the number of Communication satellite launches per year from 1960 to 2008. The first notable feature of this time series is that, unlike both the D&I and Science satellite launches, no sharp increase occurs in the yearly launches at the dawn of the space age. Instead, we notice a slow ramp up of the number of communication satellites launched per year from a low 4 in 1960 to 51 in 1976 (compare this feature with the time to peak of both D&I and Science satellites in the mid 1960). The most salient feature in Fig. 6 is the "bubble" with its sharp rise and fall between 1996 and 2001. From roughly an average of 45 communication satellites launched per year, the number increased to a dramatic 115 in 1998, and crashed to 29 in 2001. This rise and fall is due to the Low Earth Orbit (LEO) communication satellites, and in particular to the Iridium constellation, which between 1997 and 1998, launched 57 satellites [7]. Finally, it can be seen in Fig. 6 that following the "burst of the bubble", the number of communication satellites launched seems to have settled between 20 to 30 per year, at lower value than what it was before the bubble (roughly 45 per year).

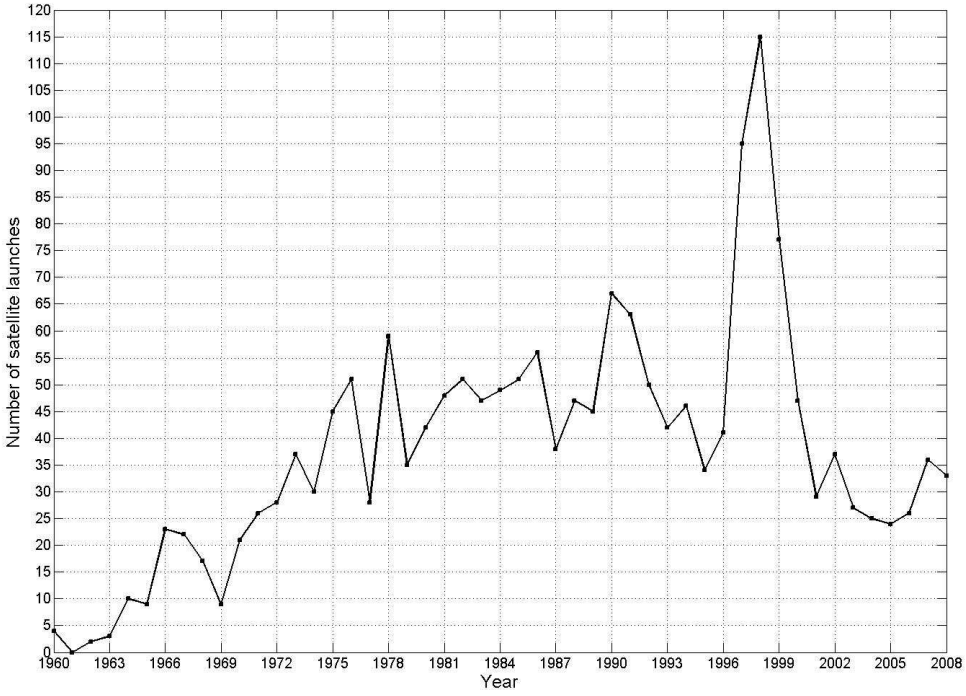

Figure 6: Communication satellite launches per year from 1960 to 2008

Following this qualitative discussion, we conduct in the following section quantitative analyses of these time series and identify local trends and cyclical patterns embedded in the data.

4. Spectral analysis of launch data and identification of cycles in the time series

In this section, we use an analytical tool, the Discrete Fourier Transform (DFT) to identify periodic components in our three time series. A brief introduction to this tool is first provided before it is put to use to analyze our data.

4.1. Discrete Fourier Transform (DFT) Presentation

The Discrete Fourier Transform (DFT), and its efficient algorithmic implementation the Fast Fourier Transform (FFT), is extensively used in signal processing to reveal periodicities in various sorts of input data (hence its characterization as a "spectral analysis" technique). The DFT also reveals the relative weight or contribution of each periodic component in the signal. The continuous

Fourier Transform converts a function of a real variable, typically in the time domain, into another function, often referred to as the frequency domain representation of the original function. The Fourier Transform identifies all the frequencies in the original function and the intensity in each infinitely small frequency interval $\omega+\delta\omega$ (see for example [8, 9] for details). The Discrete Fourier Transform achieves the same objective except that the input function (to be transformed) is discrete. There are a couple of mathematical subtleties when working with the DFT/FFT that one should be aware of before interpreting its results; these will be discussed shortly.

Mathematically, for a vector $\boldsymbol{X} = [X_0 : X_{M-1}]$ of M real values, the DFT vector $\boldsymbol{F} = [F_0 : F_{N-1}]$, computed in N points ($N \geq M$), is expressed as follows [9]:

$$F_p = \sum_{j=0}^{N-1} X_j \omega_n^{\,jp} \qquad \text{with} \qquad p = [0 ; N-1] \tag{1}$$

where

$$\omega_n = \exp\left(-\frac{2\pi i}{N}\right) \qquad \text{with} \qquad i^2 = -1 \tag{2}$$

Data in the input vector $\boldsymbol{X}$ are separated by a constant interval in time, $\Delta t = 1/f_s$, where f_s is the sampling frequency. The DFT of $\boldsymbol{X}$ is the output vector $\boldsymbol{F}$, and its components F_p are complex-valued. For, $p \in [0 ; N-1]$, $|F_p|$ measures the amplitude of the component in the signal at the frequency $f = p \times \frac{f_s}{N}$.

The Discrete Fourier Transform is well suited for the purpose of the present work since the cycles, if any, we wish to identify in the time series are periodic components that would appear in the frequency domain representation (or the discrete Fourier transform) of the time series. In addition, a time series being by definition a discrete vector, the DFT is by design suited for handling such data format.

The choice of the number of points N on which the DFT is computed is of special importance. Recall that M is the length of the input vector, and N of the length output vector. $N = M$ is sometimes used, but more often the DFT is computed on more points than in the initial vector. The method for doing so is referred to as "zero-padding" and consists of appending an array of zeros to the end of the input signal, thus extending the discrete input signal before the DFT is applied. Zero-padding is extensively used in practice, mainly because it yields finer "resolution" in the spectral domain (to be precise, zero-padding provides higher interpolation density in the frequency domain). Additional details on the DFT, FFT, and zero-padding can be found in [8,10]. In the remainder of this chapter, we use the typical value $N = 2M$, that is the zero-padding doubles the length of original input vector (the implication of this choice will be highlighted when discussing the periodograms of the time series). Our input vectors, the number of satellites launched per year from 1960 to 2008, have a length $M = 49$. Given our choice of N ($2M = 98$ points) and the way the DFT is computed, two particular frequencies will appear in the periodogram as numerical artifacts. These will be further discussed in the following subsection. In the following, we define the time vector $\mathbf{t} = [1960: 2008]$ with components t_j for the spectral analysis.

4.2. D&I satellites: Spectral analysis, harmonic modeling and residual analysis

4.2.1. Spectral analysis

The first step of the spectral analysis consists of removing the offset or dc component in each time series. This means subtracting the average of the input vector before applying the DFT. Let **X** be the initial vector, of size M, of the number of D&I satellite launches per year, from 1960 to 2008, we first calculate:

$$\langle X \rangle = \frac{1}{M} \sum_{j=0}^{M-1} X_j \tag{3}$$

For the D&I satellites, $\langle X \rangle = 45.7$ launches per year. We then define a new vector $\mathbf{Y_1}$ as the shifted version of **X** stripped of its average component:

$$Y_{1,j} = X_j - \langle X \rangle \quad \text{for } j = [0 : M-1]$$

thus (4)

$$\langle Y \rangle = 0$$

The DFT is next applied to the new vector $\mathbf{Y_1}$ in N points, and the cyclical content or harmonic components in this vector, if any, will be revealed by its periodogram. The periodogram of an input vector consists of a plot of power versus frequency, that is, a representation of the power in each frequency component of the input vector. The x-axis of the periodogram represents a frequency range given by Eq. 5:

$$f = p \times \frac{f_s}{N} \tag{5}$$

$$\text{with} \begin{cases} p = [0 : N-1] \\ f_s = \dfrac{samples}{unit\ time} = 1/\ year \end{cases}$$

The y-axis of the periodogram represents the power in each frequency component of the input vector, and is calculated as follows:

$$Power[DFT(\mathbf{Y_1})] = \frac{DFT(\mathbf{Y_1}) \times \overline{DFT(\mathbf{Y_1})}}{N} \tag{6}$$

$\overline{DFT(\mathbf{Y_1})}$ is a vector with components that are the complex conjugates of the components of the $DFT(\mathbf{Y_1})$ vector. The product in Eq. 6 in effect provides us with the square of the amplitude of each component (complex number) of the DFT. The periodogram of $\mathbf{Y_1}$ is provided in Fig. 7.

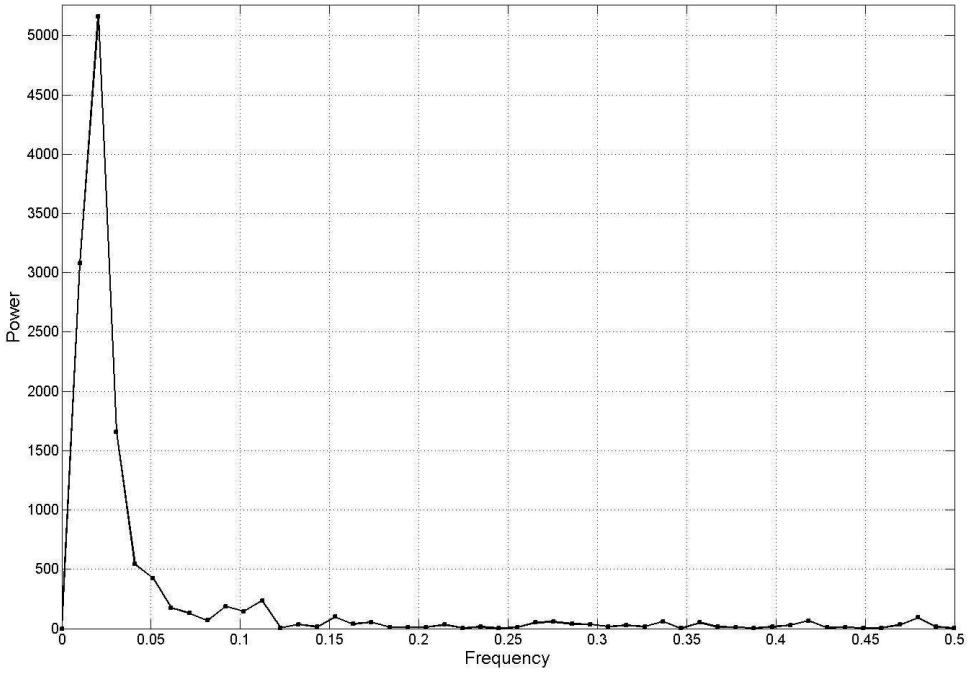

Figure 7: Periodogram of $\mathbf{Y_1}$

We notice first the main peak in the periodogram of $\mathbf{Y_1}$ at the frequency is $f_1 \cong 0.02041$. This frequency corresponds to a cycle with a period T_1:

$$T_1 = \frac{1}{f_1} = 49 \; years$$

This result is the numerical artifact referred to previously, and it derives from the length of our input vector* and the way the DFT is computed. This first cyclical component is modeled as follows:

$$a_1 \times \cos\left(\frac{2\pi}{T_1}\boldsymbol{t} + b_1\right) \tag{7}$$

The coefficients a_1 and b_1 are derived using the least-square method (a_1 = -29.03, b_1 = 0.8871). The result of Eq. 7 and $\mathbf{Y_1}$ are shown in Fig. 8.

* Time series with 49 yearly data points form 1960 till 2008.

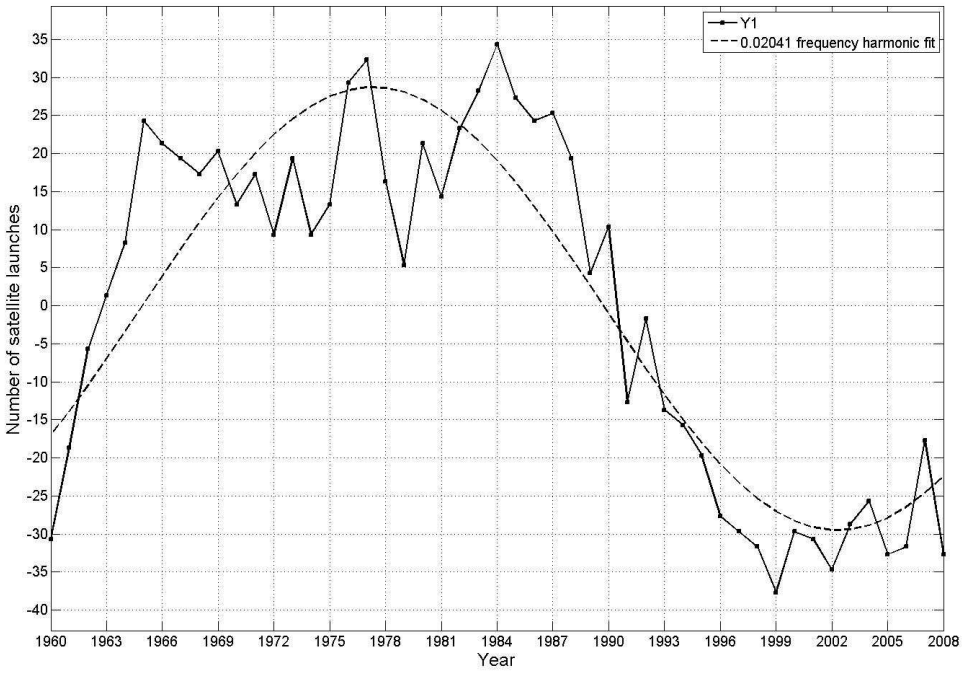

Figure 8: $\mathbf{Y_1}$ and the first cyclical component at $\mathbf{T_1}$ = 49 years ($\mathbf{f_1}$=0.02041)

Unfortunately, this harmonic component (with T_1 = 49 years) is significantly dominant and "drowns" the contributions of other possible harmonic components in the input vector as can be seen in the periodogram in Fig. 7. In order to distinguish other possible cycles in the time series, we proceed by filtering out this single frequency in the signal—for a parallel with signal processing, this action can be thought of as a highly selective notch filter—and re-apply the DFT to the signal stripped of its average component and of the harmonic component with a T_1 period. In short, we create a new vector $\mathbf{Y_2}$ such that:

$$Y_{2,j} = Y_{1,j} - a_1 \times \cos\left(\frac{2\pi}{T_1} t_j + b_1\right) \quad \text{for } j = [0 : M-1] \tag{8}$$

The new vector $\mathbf{Y_2}$ is shown in Fig. 9, and its periodogram is provided in Fig. 10.

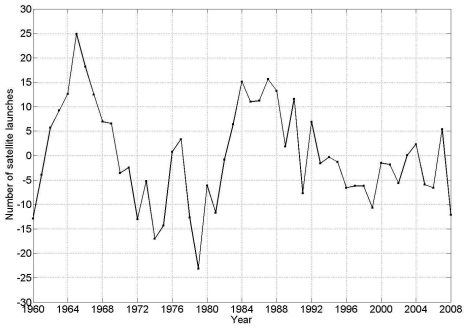

Figure 9: $\mathbf{Y_2}$ vector

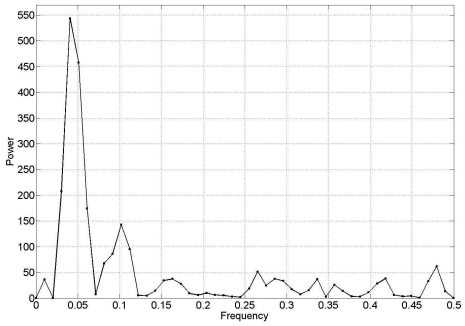

Figure 10: Periodogram of $\mathbf{Y_2}$

Having eliminated the dominant harmonic component (at T_1) from the input vector, we notice that the new periodogram of $\mathbf{Y_2}$ provides more information about the frequency content in the new signal as more peaks appear than what was initially present in Fig. 7. Still however, one dominant peak is visible in Fig. 10 and it occurs at $f_2 \cong 0.04082$. This frequency corresponds to a cycle with a period T_2:

$$T_2 = \frac{1}{f_2} = 24.5 \; years$$

This result is also a numerical artifact, referred to previously, and it derives from both the length of our input vector and our choice of the length of zero-padding. This second cyclical component is modeled as follows:

$$a_2 \times \cos\left(\frac{2\pi}{T_2}\boldsymbol{t} + b_2\right) \tag{9}$$

As with the first cyclical component, the coefficients a_2 and b_2 are derived using the least-square method (a_2 = 9.42, b_2 = -1.086). The result of Eq. 9 and $\mathbf{Y_2}$ are shown in Fig. 11.

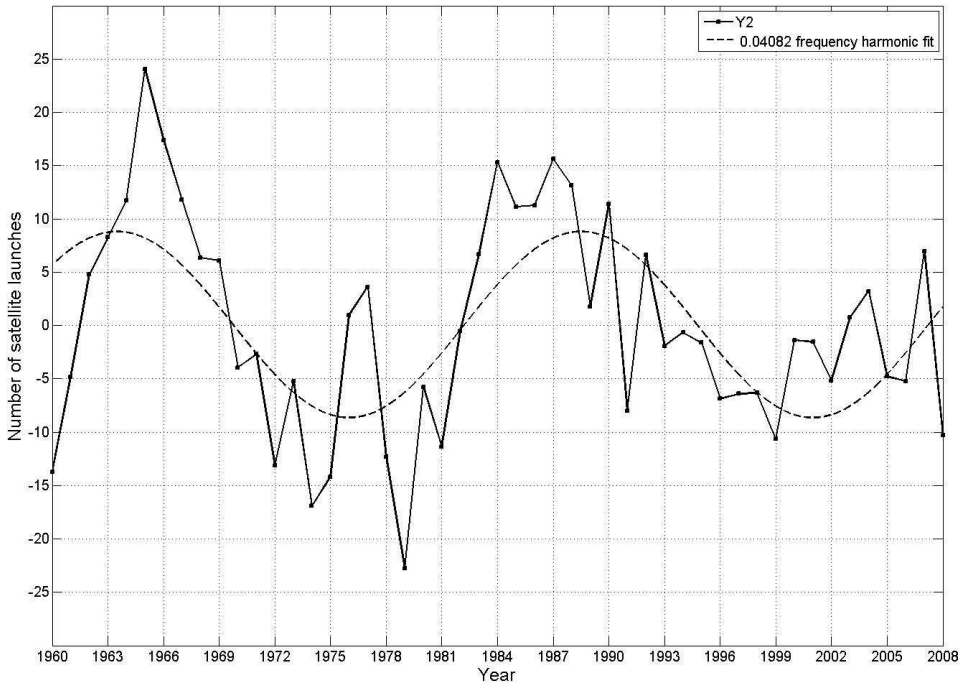

Figure 11: Y_2 and the second cyclical component at T_2 = 24.5 years (f_2=0.04082)

The new vector $\mathbf{Y_3}$ is created, from the original raw data, stripped of the average component $\langle X \rangle$ and the two numerical artifacts that dominated the periodogram of the time series and drowned the cyclical content of the signal:

$$Y_{3,j} = Y_{2,j} - a_2 \times \cos\left(\frac{2\pi}{T_2} t_j + b_2\right) \quad \text{for } j = [0 : M-1] \tag{10}$$

The new vector $\mathbf{Y_3}$ is shown in Fig. 12, and its periodogram is provided in Fig. 13.

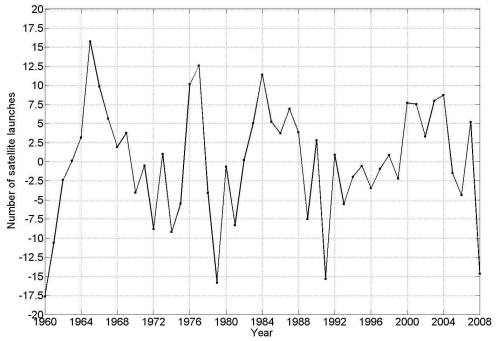

Figure 12: Y_3 vector

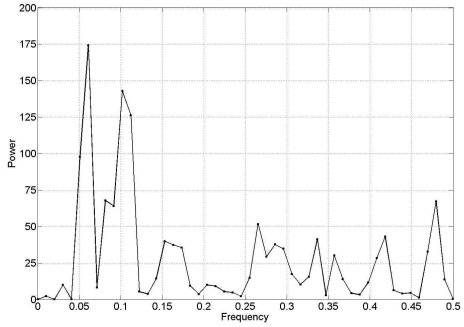

Figure 13: Periodogram of Y_3

Having eliminated the two dominating frequencies f_1 = 0.02041 and f_2 = 0.04082 (the harmonic components with periods T_1 = 49 years, and T_2 = 24.5 years) from the input signal, the actual frequency content of the time series now emerges quite clearly, as shown in the periodogram in Fig. 13.

We identify in the periodogram of $\mathbf{Y_3}$ several cyclical components. These components are provided next by decreasing order of their power content, and the parameters of these harmonic components a_i and b_i (similar to Eq. 7 and 9) are provided in Table 2.

- $f_3 \cong 0.06122$ and $f_4 \cong 0.102$, which correspond to two cycles with periods of:

$$\begin{cases} T_3 = \dfrac{1}{f_3} \cong 16.3 \; years \\ T_3 = \dfrac{1}{f_4} \cong 9.8 \; years \end{cases}$$

- $f_5 \cong 0.08163$, $f_6 \cong 0.2653$, $f_7 \cong 0.4796$, $f_8 \cong 0.1633$ and $f_9 \cong 0.2857$, which correspond to cycles with periods of:

$$\begin{cases} T_5 \cong 12.3 \; years \\ T_6 \cong 3.8 \; years \\ T_7 \cong 2.1 \; years \\ T_8 \cong 6.1 \; years \\ T_9 \cong 3.5 \; years \end{cases}$$

A summary of all harmonic components in the time series of the D&I satellite launches is provided in Table 2, organized in a three-tier grouping: Tier 1 contains the two numerical artifact cycles (periods T_1 = 49 years, and T_2 = 24.5 years); Tier two contains the second most dominant cycles in the time series (T_3 = 16.3 years, and T_4 = 9.8 years). Tier 3 contains the remaining cycles.

Table 2: D&I satellites category spectral analysis results

	Cycle number i	*Period T_i (years)*	*Frequency f_i*	a_i	b_i
Tier 1	***1***	**49.0**	0.0204	-29.03	0.8871
	2	**24.5**	0.0408	9.42	-1.0860
Tier 2	***3***	**16.3**	0.0612	-5.33	0.1496
	4	**9.8**	0.1020	-4.82	0.1591
Tier 3	***5***	**12.3**	0.0816	-3.33	0.7161
	6	**3.8**	0.2653	-2.90	0.4656
	7	**2.1**	0.4796	-2.98	0.4094
	8	**6.1**	0.1633	2.49	1.4990
	9	**3.5**	0.2857	2.50	2.5380

The harmonic model $\mathbf{H_{D\&I}}$ approximating the time series of D&I satellite launches can be written as follows (the numerical values of the parameters are those in Table 2):

$$H_{D\&I,j} = \langle X \rangle + \sum_{k=1}^{9} a_k \times \cos\left(\frac{2\pi}{T_k} t_j + b_k\right) \qquad \text{for} \quad j = [0 : M-1] \tag{15}$$

The result of the harmonic modeling and the D&I time series is shown in Fig. 14. A quick visual inspection indicates a suitable fit of the data, and no conspicuous inaccuracies in the results of our multi-stage approach with Fourier analysis and notch-filtering. A quantitative analysis of the quality of fit and error residual between the raw data and the harmonic model is provided next.

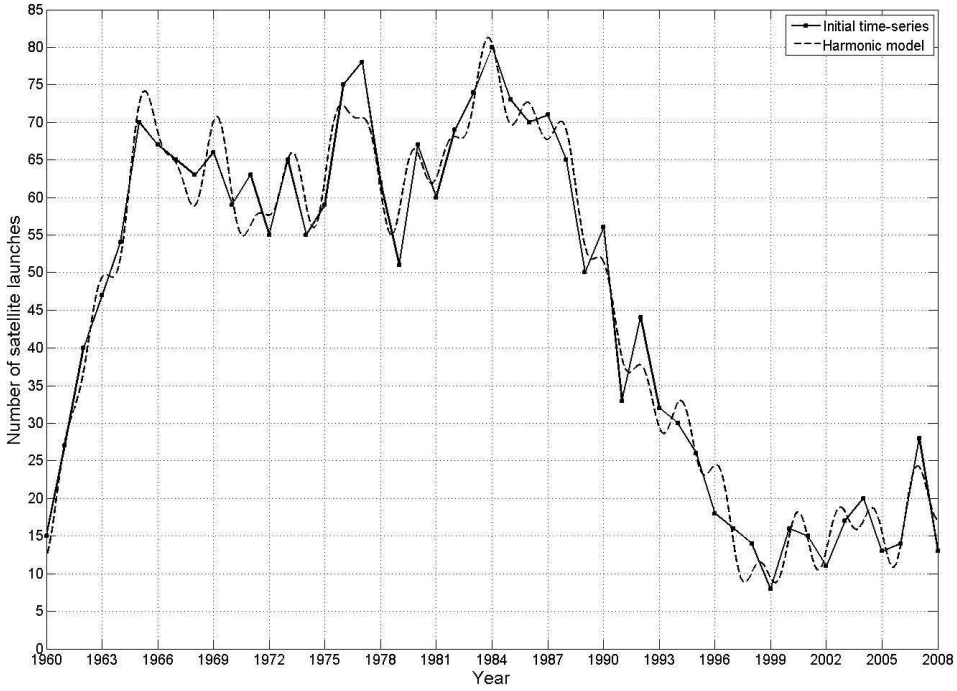

Figure 14: D&I satellite time series and its harmonic model

4.2.2. Error analysis

Given the initial time series $\boldsymbol{X}$ and its harmonic model $\boldsymbol{H_{D\&I}}$, the residual error $\boldsymbol{R}$ is the difference between each component of the two vectors:

$$R_j = X_j - H_{D\&I,j} \qquad \text{for j} = [0 : \text{M} - 1] \tag{16}$$

The residual error of the D&I satellites category is shown in Fig.15. The average of the residual is 0 (confirming proper numerical calculations) and its standard deviation 3.38, which represents roughly 7% of the average launches of D&I satellites between 1960 and 2008.

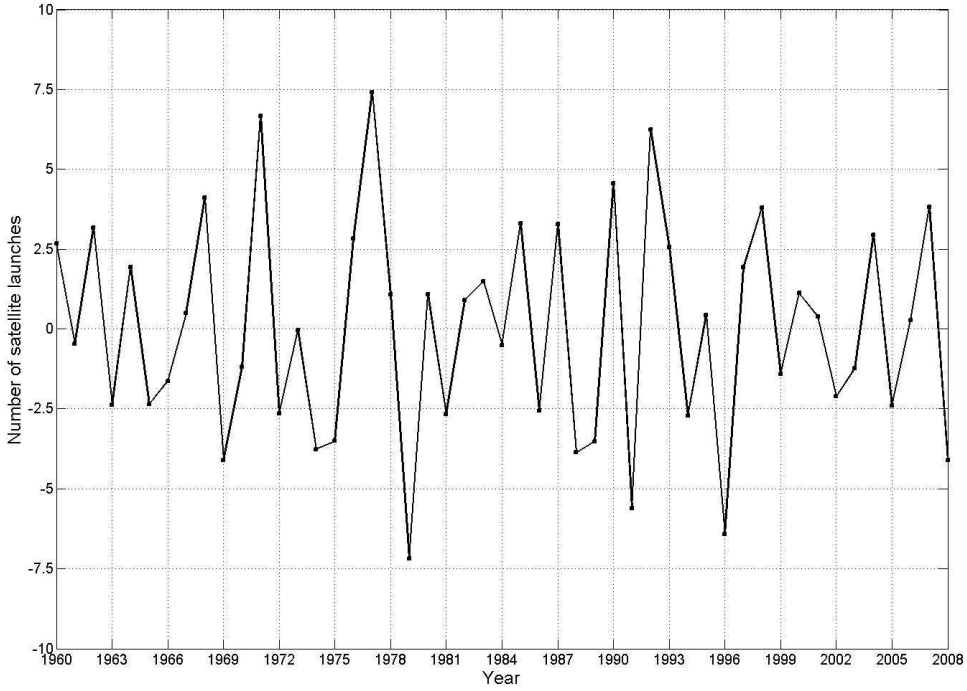

Figure 15: Residual error for the D&I satellites category

While more accuracy can be obtained by increasing the number of cycles in the harmonic model, the important statistic from the residual analysis, beyond the average and standard deviation, is the actual distribution from which these data points arise, for reasons discussed next. Different statistical analysis techniques are available for determining the appropriate parametric distribution the data is likely to arise from. The more convenient and expeditious method is a set of graphical techniques known as probability plotting. For example, the Normal Probability plot is used to assess whether data arises from a normal distribution. Other plots, for example the Weibull and lognormal plots are used to assess whether the data arise for said distributions. The general idea of probability plotting is that under specific mathematical transformation for each parametric distribution, the data should be aligned (linear) in the plot with the new variables for axes, if the data indeed arises from the distribution under study. If the data points are not aligned in the probability plot of a distribution *D*, it can be concluded that distribution *D* is unfit to model the data (i.e., the data does not arise from distribution *D*). Details about the Weibull plot can be found in [11] and the normal plot in [12]. The normal plot of the residual error for the D&I satellite category is provided in Fig.16.

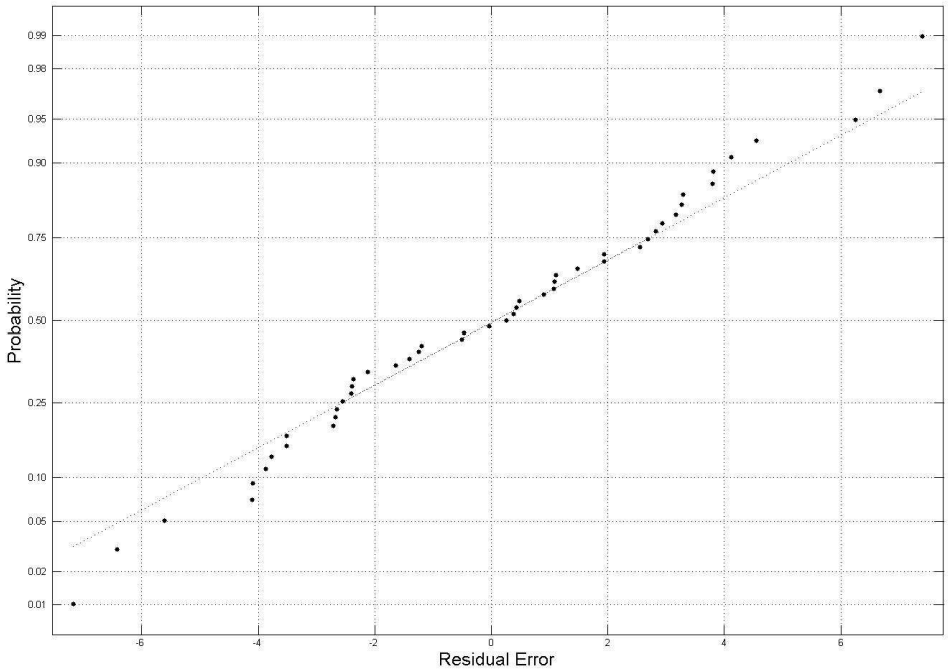

Figure 16: Normal plot of the residual error for the D&I satellite category

The results in Fig. 16 are well aligned. In order to analytically support the normality hypothesis, we conducted the following correlation analysis. The proposed test statistic, the normal probability plot correlation coefficient *r*, is defined as the product moment correlation coefficient between the ordered observations and the order statistic medians from a normal $N(0,1)$ distribution [13]. Underlying normality will yield a linear normal probability plot, which in turn will be reflected by unity value of the probability plot correlation coefficient *r*. For the residual error of the D&I satellites category, our analysis provided a normal probability plot correlation coefficient r = 0.995. This result is a good indication that the Normal distribution is indeed appropriate and that the error residuals can be modeled with reasonable accuracy by a Normal distribution. The probability density function $f_{D\&I}(x)$ of this normal distribution is provided in Eq. 17:

$$\begin{cases} f_{D\&I}(x) = \dfrac{1}{\sigma\sqrt{2\pi}} \exp\left[-\dfrac{(x-\mu)^2}{2\sigma^2} \right] \\ \text{mean } \mu = 0 \\ \text{stdev } \sigma = 3.4 \end{cases} \tag{17}$$

It should be noted that a trade-off exists between the value of the standard deviation of the normal distribution of the error residuals and the number of cycles identified and considered in the harmonic model of the time series (more cycles result in a smaller standard deviation for the residual distribution). In addition, for forecasting purposes as done in Section 5, we re-derive harmonic and residual models based on time series data from the last decade only (not extending back to 1960).

In the following subsections, we provide the corresponding results for the two remaining time series, the Science satellites and the Communication satellites. The steps of the analysis are similar to the ones detailed for the D&I satellites, and will not be repeated hereafter.

4.3. Science satellites: Spectral analysis, harmonic modeling and residual analysis

As with the D&I satellites, 9 cycles have been identified for the Science satellites category. The results are provided in Table 3.

Table 3: Science satellites category spectral analysis results

	Cycle number i	***Period T_i (years)***	***Frequency f_i***	***a_i***	***b_i***
Tier 1	***1***	**49.0**	0.0204	-13.93	0.9126
	2	**24.5**	0.0408	11.73	1.5560
Tier	***3***	**31.6**	0.0316	-8.14	12.1500

2	***4***	**12.3**	0.0810	-4.09	0.9193
Tier 3	***5***	**3.4**	0.2959	-3.97	0.5730
	6	**16.4**	0.0610	3.84	-0.3049
	7	**6.1**	0.1633	3.20	1.6540
	8	**2.0**	0.4898	-2.94	0.8577
	9	**3.1**	0.3265	-2.71	-5.0430

The harmonic model $\mathbf{H_{sci}}$ approximating the time series of Science satellite launches can be written as follows (the numerical values of the parameters are those in Table 3):

$$H_{sci,\,j} = \langle X \rangle + \sum_{k=1}^{9} a_k \times \cos\left(\frac{2\,\pi}{T_k}\, t_j + b_k\right) \qquad \text{for } j = [0 : M-1] \tag{18}$$

The result of the harmonic modeling and the Science time series is shown in Fig. 17. A quick visual inspection indicates a suitable fit of the data. A quantitative analysis of the error residual is provided next.

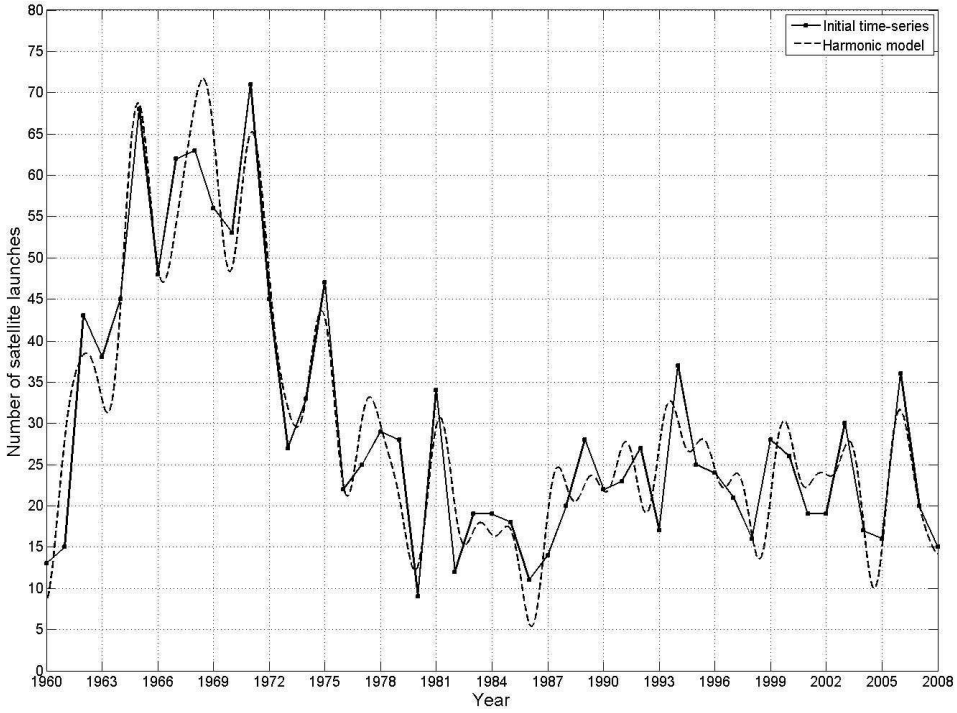

Figure 17: the Science satellite category time-series and its harmonic model

The residual error of the Science satellites category is illustrated in Fig. 18. The average is 0 and the standard deviation of the error is 4.8. The normal plot of the residual error for the Science satellites is presented in Fig. 19.

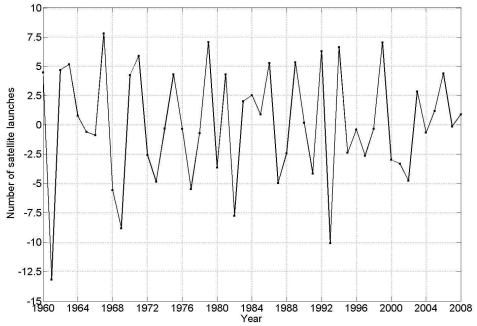

Figure 18: Residual error

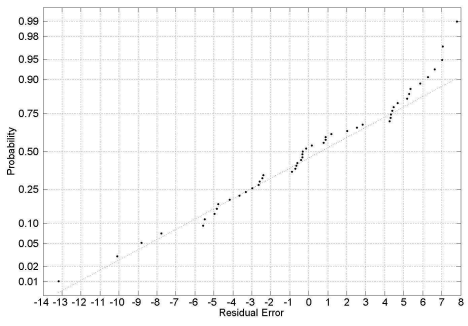

Figure 19: Normal plot of the residual error

The results in Fig. 19 are well aligned, and a correlation analysis provides a normal probability plot correlation coefficient r = 0.985. This result is again a good indication that the Normal distribution

is indeed appropriate and that the error residuals for the Science satellites can be modeled with reasonable accuracy by a Normal distribution. The probability density function $f_{sci}(x)$ of this normal distribution is provided in Eq. 18:

$$\begin{cases} f_{sci}(x) = \dfrac{1}{\sigma\sqrt{2\pi}} \exp\left[-\dfrac{(x-\mu)^2}{2\sigma^2}\right] \\ \text{mean } \mu = 0 \\ \text{stdev } \sigma = 4.8 \end{cases} \tag{18}$$

4.4. Communication satellites: Spectral analysis, harmonic modeling and residual analysis

As with the two other satellites categories, 9 cycles have been identified for the Communication satellite category. They are identified in Table 4.

Table 4: Communication satellites category spectral analysis results

	Cycle number i	***Period T_i (years)***	***Frequency f_i***	***a_i***	***b_i***
Tier 1	***1***	**49.0**	0.0204	22.30	1.2540
	2	**24.5**	0.0408	9.85	0.2033
Tier 2	***3***	**8.2**	0.1224	-10.59	11.8600
	4	**9.8**	0.1020	6.92	1.4210
Tier 3	***5***	**6.7**	0.1497	6.29	-0.3087
	6	**4.5**	0.2245	-5.63	-0.5463
	7	**12.3**	0.0816	5.32	-0.5854
	8	**5.8**	0.1735	-4.66	-0.3155
	9	**5.2**	0.1939	-4.18	1.0860

The harmonic model $\mathbf{H_{com}}$ approximating the time series of Communication satellite launches can be written as follows (the numerical values of the parameters are those in Table 4):

$$H_{com,j} = \langle X \rangle + \sum_{k=1}^{9} a_k \times \cos\left(\frac{2\pi}{T_k} t_j + b_k\right) \qquad \text{for } j = [0 : M-1] \tag{19}$$

The result of the harmonic modeling and the Communication time series is shown in Fig. 20.

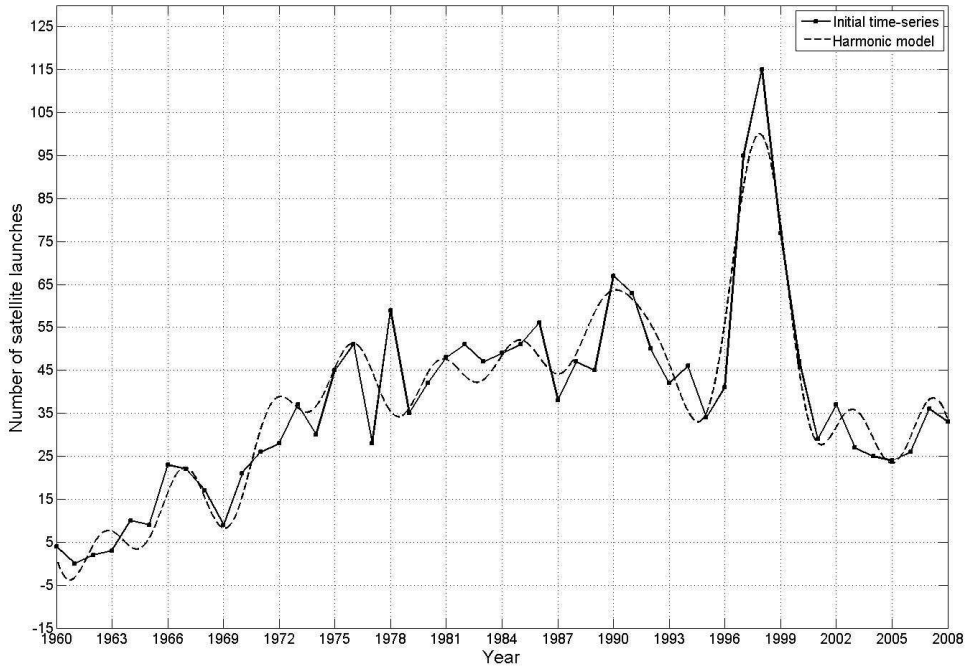

Figure 20: the Communication satellite category time-series and its harmonic model

The residual error of the Communication satellites category is shown in Fig. 21. The average is 0 and the standard deviation of the error is 7.1. The normal plot of the residual error for the Communication satellites category is presented in Fig. 22.

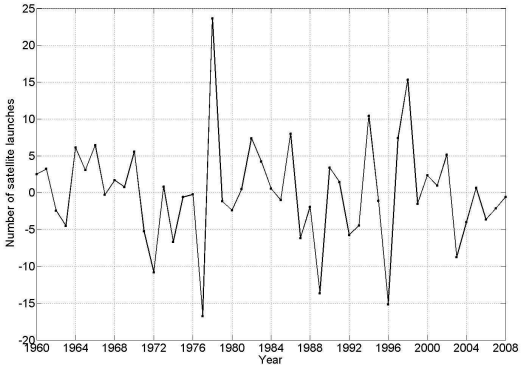

Figure 21: Residual error

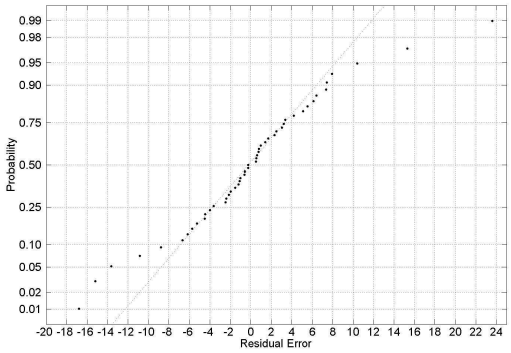

Figure 22: Normal plot of the residual error

Figures 21 and 22 show two "anomaly periods" in the launch of communication satellites, the first between 1977 and 1978, and the second one between 1996 and 1998. These "anomalies" reflect the inability of the harmonic model to properly follow the actual time series during these periods resulting in discrepancy or bias, as shown in the data points away from the "normal line" in Fig. 22. The normal probability plot coefficient of correlation is more degraded that of the previous satellite categories, but remains nevertheless significantly high with r = 0.970. This result supports the hypothesis that the residual error between the initial time series and the harmonic model can be modeled with reasonable accuracy by a Normal distribution. However, for forecasting purposes, as discussed in the next section, we will derive a new harmonic model that does not extent back in time to include these two anomalous periods.

5. Forecasting satellite launch volume

The objective of this section is to forecast the launch volume of satellites in each category for the next four years (2009–2012). For practical and conceptual reasons, we re-derive harmonic models based on spectral analysis of the time series restricted to roughly the last decade (instead of extending back to 1960).

5.1. D&I satellites

Figure 23 shows the number of D&I satellite launches each year from 1998 to 2008. The periodogram of this time series, stripped of its average component is provided in Fig. 24.

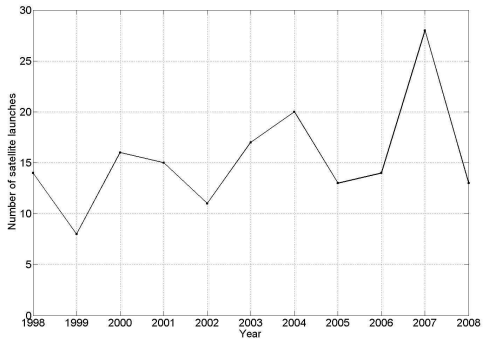

Figure 23: D&I satellite launches per year from 1998 to 2008

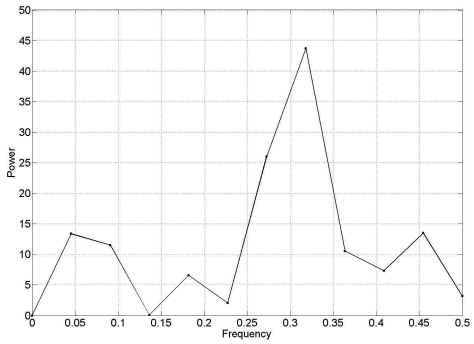

Figure 24: Periodogram

The most dominant frequency in this time series is $f_1 \cong 0.3182$, which corresponds to a period T_1 = 3.1 years. Two secondary frequencies are also identified in a manner similar to the one discussed in Section 4. The results are shown in Table 5.

Table 5: D&I satellite category spectral analysis results (restricted to the period 1998/2008)

	Cycle number i	***Period T_i (years)***	***Frequency f_i***	***a_i***	***b_i***
Dominant cycle	***1***	3.1	0.3182	-5.64	5.792
Secondary cycles	***2***	2.2	0.4545	-3.13	-3.987
	3	22.0	0.0454	-3.21	-10.980

The resulting harmonic model $\mathbf{H_{D\&I}}$ fitting the D&I time series restricted from 1998 to 2008 is expressed as follows:

$$H_j = \langle X \rangle + \sum_{k=1}^{3} a_k \times \cos\left(\frac{2\pi}{T_k} t_j + b_k\right) \qquad \text{for } j = [0 : M-1] \tag{22}$$

Its parameters are provided in Table 5, and the results are shown in Fig. 25.

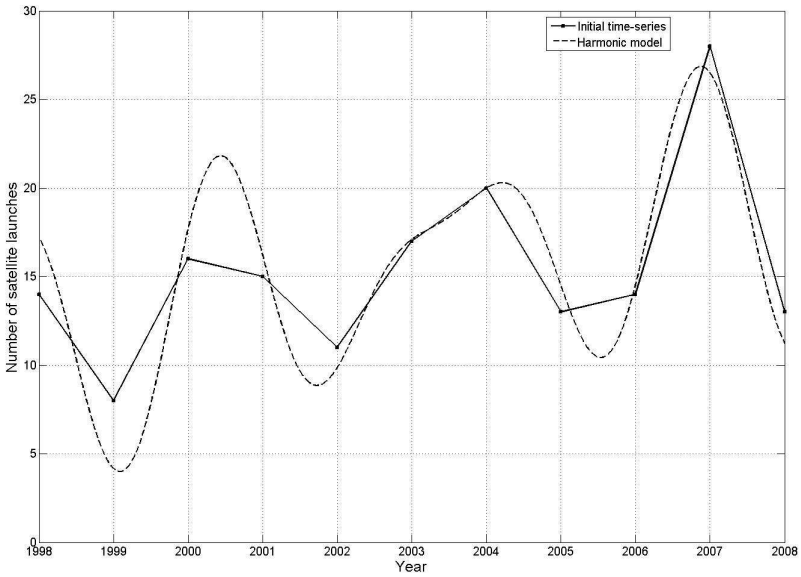

Figure 25: 11-years D&I satellite category time series and its harmonic model

We then compute the residual error **R** between the time series and the new harmonic model. The average error is 0 and its standard deviation is 2.0. The normal plot of the residuals is shown on Fig. 26. The results are well aligned, and a correlation analysis provides a normal probability plot correlation coefficient r = 0.985. This result is again a good indication that the Normal distribution is indeed appropriate and that the residuals can be modeled with reasonable accuracy by a Normal distribution.

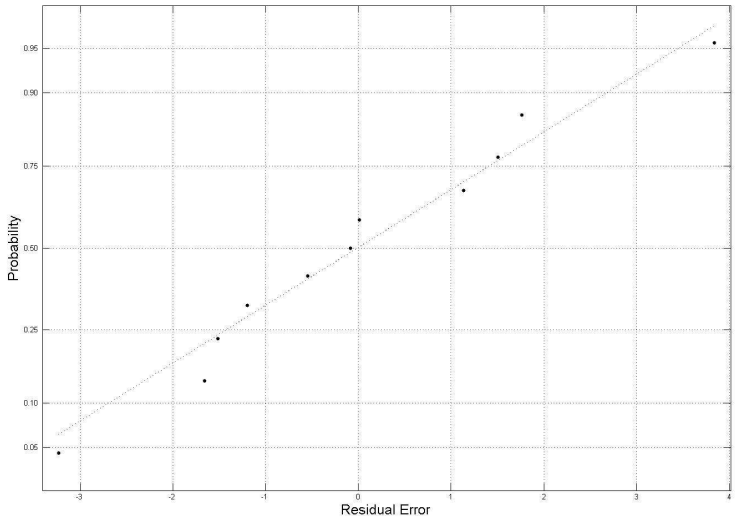

Figure 26: Normal plot of the residual error R

To build the forecasting model, the harmonic model $\mathbf{H_{D\&I}}$ is extended from 2009 to 2012, and a probabilistic error component is added to it. The error model is normally distributed with the parameters derived previously from the normal plot of the residuals. As a result, we can derive the 95% confidence intervals of the satellite launch volume (assuming stationarity). The forecasting model for the D&I category is shown in Fig. 27, and the data are provided in Table 6.

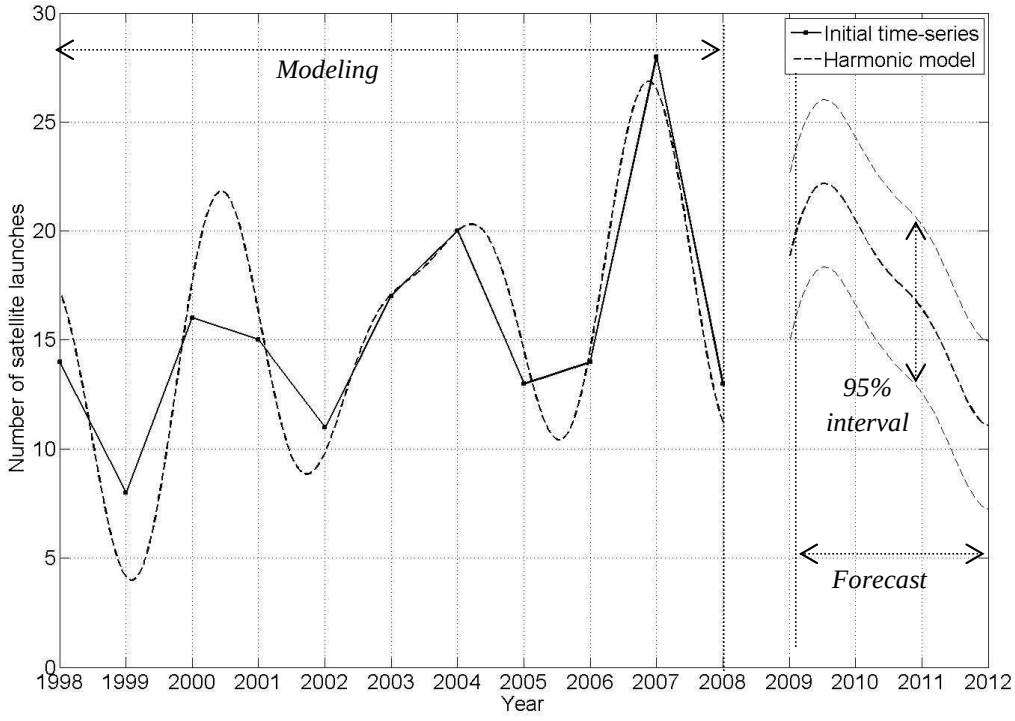

Figure 27: D&I satellite forecasting results with 95% confidence intervals

Table 6: Forecasted volume of D&I satellite launches

Year		**2009**	**2010**	**2011**	**2012**
Baseline (rounded)		19	21	16	11
95% confidence interval (rounded)	**Upper bound**	23	24	20	15
	Lower bound	15	17	13	7

5.2. Science satellites

Figure 28 shows the number of Science satellite launches each year from 1998 to 2008. The periodogram of this time series, stripped of its average component is provided in Fig. 29.

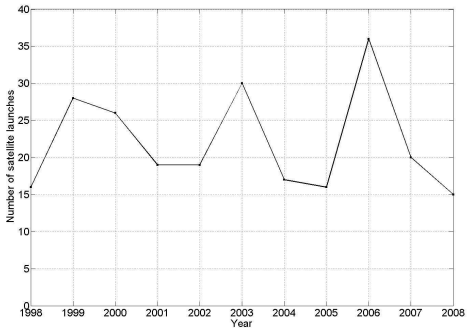

Figure 28: Science satellite launches per year from 1998 to 2008

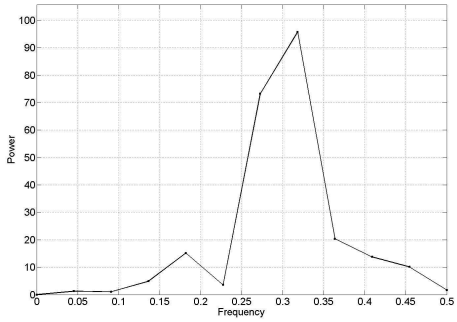

Figure 29: Periodogram

The most dominant frequency in this time series is $f_1 \cong 0.3182$, which corresponds to a period T_1 = 3.1 years. Again, two secondary frequencies are also identified in a manner similar to the one discussed in Section 4. The results are shown in Table 7.

Table 7: Science satellite category spectral analysis results (restricted to the period 1998/2008)

	Cycle number i	***Period T_i (years)***	***Frequency f_i***	***a_i***	***b_i***
Dominant cycle	***1***	3.1	0.3182	-8.54	-5.161
Secondary cycles	***2***	2.4	0.4091	3.18	1.882
	3	3.6	0.2727	1.93	-0.131

The resulting harmonic model $\mathbf{H_{Sci}}$ fitting the Science time series restricted from 1998 to 2008 is expressed as follows:

$$H_j = \langle X \rangle + \sum_{k=1}^{3} a_k \times \cos\left(\frac{2\pi}{T_k} t_j + b_k\right) \qquad \text{for } j = [0 : M-1] \tag{22}$$

Its parameters are provided in Table 7, and the results are shown in Fig. 30.

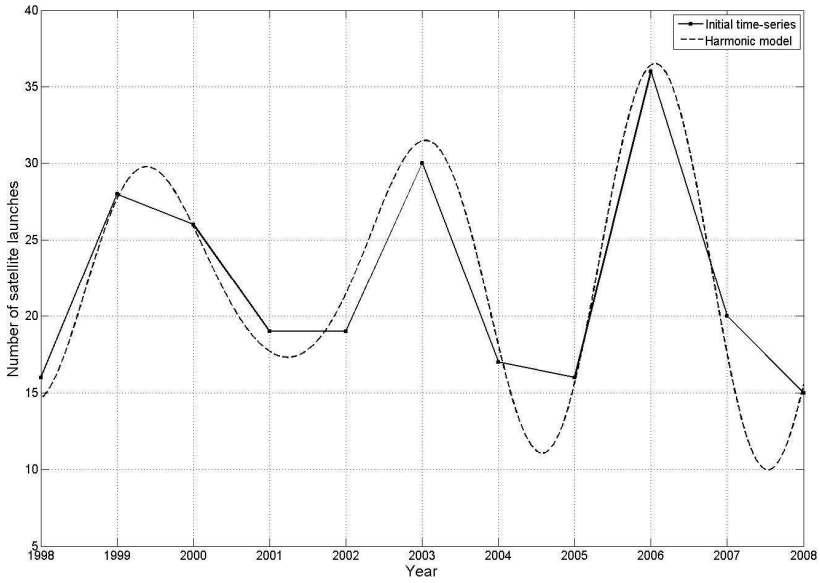

Figure 30: 11-years Science satellite category time series and its harmonic model

We then compute the residual error **R** between the time series and the new harmonic model. The average error is 0 and its standard deviation is 1.4. The normal plot of the residuals is shown on Fig. 31. The results are well aligned, and a correlation analysis provides a normal probability plot correlation coefficient r = 0.992. This result is again a good indication that the Normal distribution is indeed appropriate and that the residuals can be modeled with reasonable accuracy by a Normal distribution.

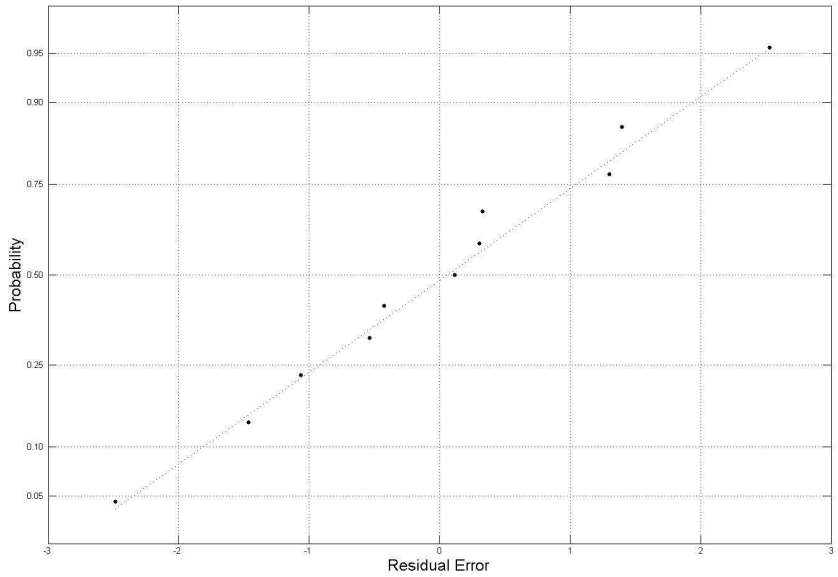

Figure 31: Normal plot of the residual error R

To build the forecasting model, the harmonic model $\mathbf{H_{Sci}}$ is extended from 2009 to 2012, and a probabilistic error component is added to it. The error model is normally distributed with the parameters derived previously from the normal plot of the residuals. As a result, we can derive the 95% confidence intervals of the satellite launch volume (assuming stationarity). The forecasting model for the Science category is shown in Fig. 32, and the data are provided in Table 8.

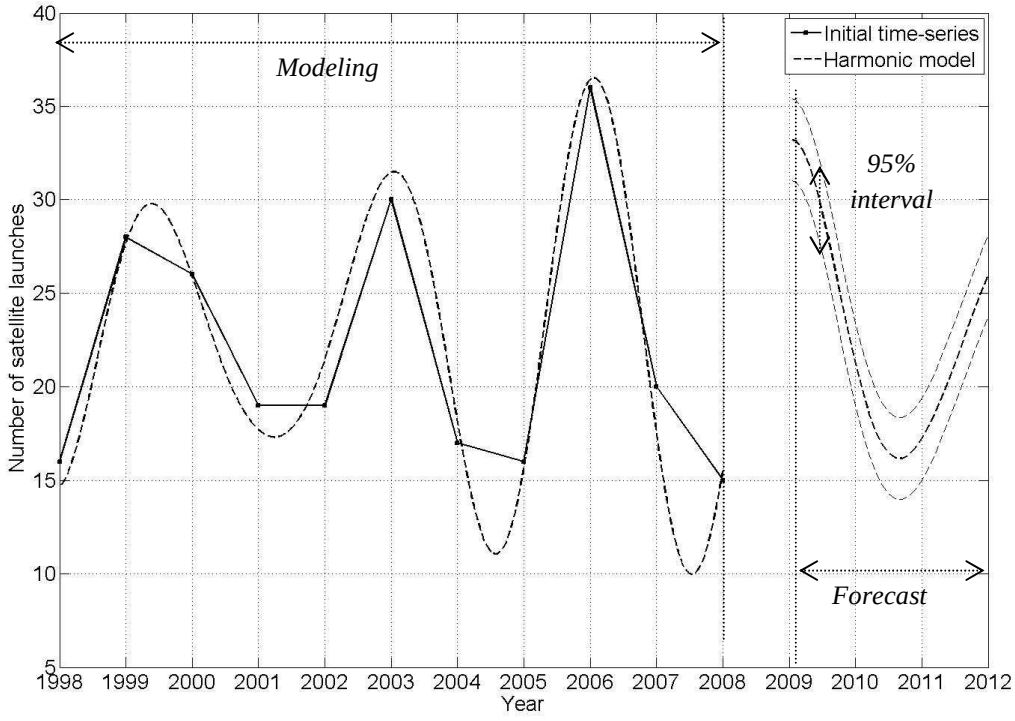

Figure 32: Science satellite forecasting results with 95% confidence intervals

Table 8: Forecasted volume of Science satellite launches

Year		**2009**	**2010**	**2011**	**2012**
Baseline (rounded)		33	21	17	26
95% confidence interval (rounded)	**Upper bound**	35	23	19	28
	Lower bound	31	19	15	24

5.3. Communication satellites category

Regarding to the Communication satellites category, the spectral analysis is achieved using the same process than for the two other categories. Yet, the time series has been restricted to the period 2001/2008; we then use a new time vector **t** = [2001:2008] in this section. The main purpose for

doing this is to filter out the Iridium Constellation anomaly, which occurs between 1996 and 2001 (see Fig. 6). We believe such anomaly is unlikely to occur again in the next few years.

Figure 33 shows the number of Communication satellite launches each year from 1998 to 2008. The periodogram of this time series, stripped of its average component is provided in Fig. 34.

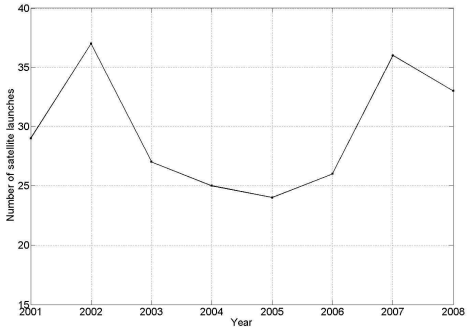

Figure 33: Communication satellite launches per year from 1998 to 2008

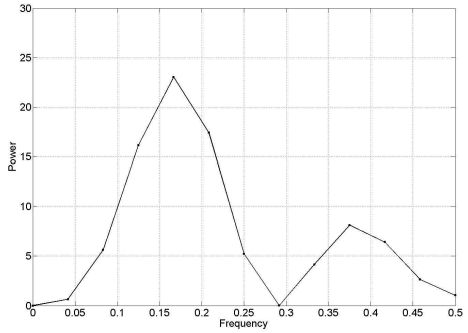

Figure 34: Periodogram

The most dominant frequency in this time series is $f_1 \cong 0.1667$, which corresponds to a period T_1 = 6.0 years. One secondary frequency is also identified. The results are shown in Table 9.

Table 9: Communication satellites category spectral analysis results (restricted to the period 2001/2008)

	Cycle number i	***Period T_i (years)***	***Frequency f_i***	***a_i***	***b_i***
Dominant cycle	***1***	**6.0**	0.1667	5.73	1.997
Secondary cycles	***2***	**2.7**	0.3750	3.49	1.707

The resulting harmonic model $\mathbf{H_{Comm}}$ fitting the Science time series restricted from 1998 to 2008 is expressed as follows:

$$H_j = \langle X \rangle + \sum_{k=1}^{2} a_k \times \cos\left(\frac{2\pi}{T_k} t_j + b_k\right) \qquad \text{for } j = [0 : M-1] \qquad (23)$$

Its parameters are provided in Table 9, and the results are shown in Fig. 35.

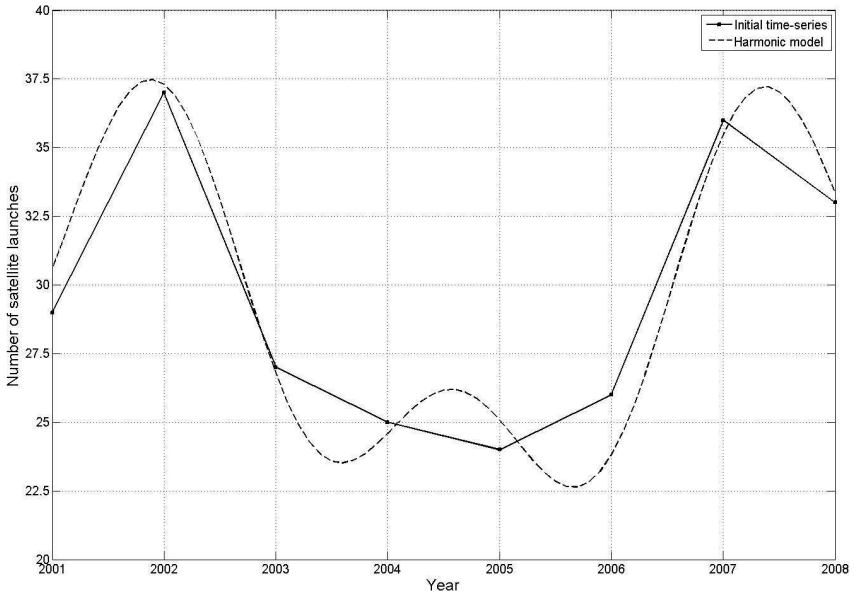

Figure 35: 8-years Communication satellite category time series and its harmonic model

The normal probability plot of the difference between the Communication satellites category time series (restricted to the 2001/2008 period) and its harmonic model is presented in Fig. 36. The results are well aligned, and a correlation analysis provides a normal probability plot correlation coefficient r = 0.967. This result is again a good indication that the Normal distribution is indeed appropriate and that the residuals can be modeled with reasonable accuracy by a Normal distribution.

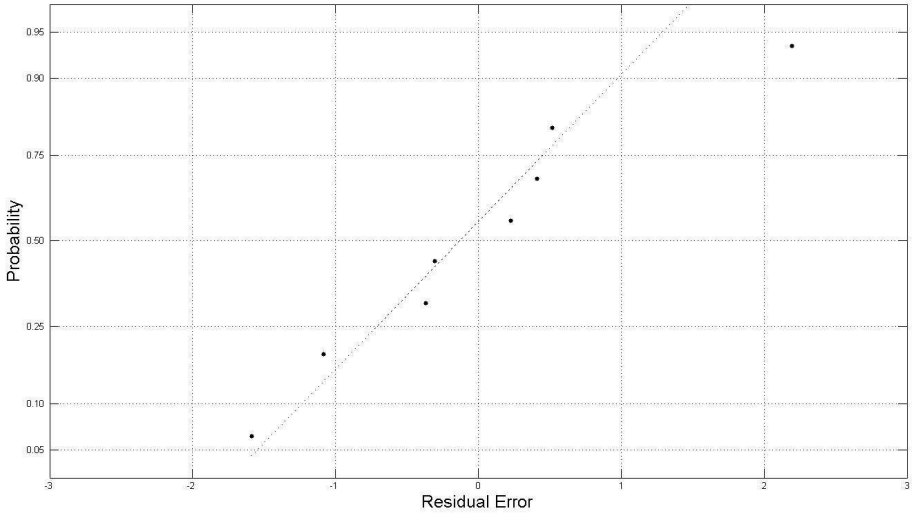

Figure 36: Normal plot of the residual error R

To build the forecasting model, the harmonic model $\mathbf{H_{Comm}}$ is extended from 2009 to 2012, and a probabilistic error component is added to it. The error model is normally distributed with the parameters derived previously from the normal plot of the residuals. As a result, we can derive the 95% confidence intervals of the satellite launch volume (assuming stationarity). The forecasting model for the Communication category is shown in Fig. 37, and the data are provided in Table 10.

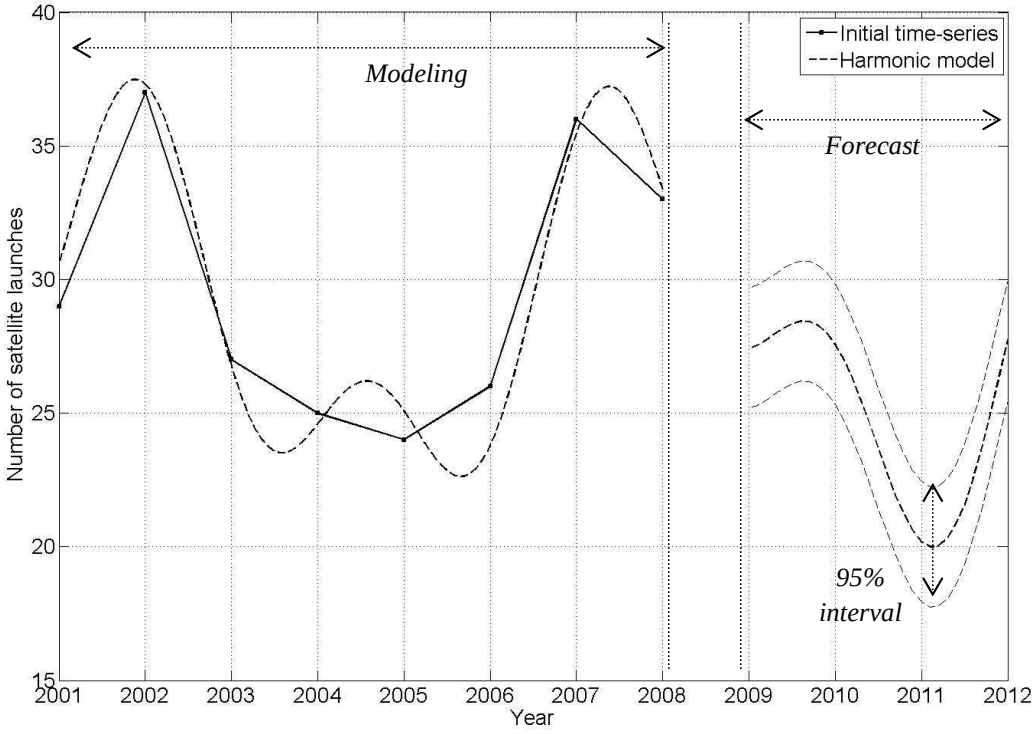

Figure 37: Communication satellite forecasting results with 95% confidence intervals

Table 10: Forecasted volume of Communication satellite launches

Year		**2009**	**2010**	**2011**	**2012**
Baseline (rounded)		27	28	20	28
95% confidence interval (rounded)	**Upper bound**	30	30	22	30
	Lower bound	25	25	18	25

6. Conclusion

Cyclicality is a feature in several industries, and its straining effects are frequently discussed and analyzed in the economic and financial literature. In addition, ways for coping with cyclicality or

mitigating its effects are often discussed in the management literature and promoted by management consultants. In the space industry, although debated occasionally, cyclicality remains largely unexplored (analytically) and its existence uncertain.

In the first chapter of this thesis, we provided an analyzed time series of satellite launches between 1960 and 2008. We identified trends and fluctuations, and clearly demonstrated the existence of cycles in satellite launch volume. Cyclicality was empirically shown across three satellite categories (and consequently three satellite *markets*): 1) Defense and Intelligence (D&I) satellites, 2) Science satellites, and 3) Communication satellites. In addition, the cycles were identified over two time periods: the entire data window (1960 to 2008), and over roughly the last decade. Distinct cycles of 3.1 years exist in launch volume for the D&I and Science satellites. The situation is a little bit more ambiguous for the communication satellites primarily because the structural anomaly in the data for this satellite category due to the Low Earth Orbit communication satellites "bubble" and its burst between 1996 and 2000. It is not yet clear how this market will evolve or settle.

It is hoped that this study be considered a small contribution toward an important topic that deserves much more attention that what it has received to date in the space industry. Satellites have been rightfully described as the lifeblood of the entire space industry and the number of satellites ordered or launched per year is an important defining metric of the industry's level of activity. The structure of the space industry, its financial health and its workforce retention and development is dependent on the volume of satellites contracted. As such, trends and cyclicality in this volume have significant strategic impact on the space industry. We hope this work invites future contributions exploring some of these issues as well as the policy drivers or levers affecting the cyclicality in the institutional markets (defense and science) and ways of handling it or mitigating its effects.

Part II: Reliability Analysis

Chapter 2: Comparative Reliability of GEO, LEO, and MEO Satellites

1. Introduction

Reliability has long been recognized as a critical attribute for space systems, and potential causes of on-orbit failures are carefully sought for identification and elimination through careful design and part selection, and extensive testing prior to launch. Unfortunately, despite the recognition of its importance, limited on-orbit failure data and statistical analyses of satellite reliability exist in the technical literature. To help fill this gap, Castet and Saleh (2009) recently collected failure data for 1,584 Earth-orbiting satellites successfully launched between January 1990 and October 2008 [14]. The authors conducted a nonparametric analysis of satellite reliability and provided empirical curves of satellite reliability with 95% confidence intervals, as presented in Fig. 38. One limitation the authors recognized and discussed in [14] is the lumping together of all Earth-orbiting satellites into one category, and statistically analyzing their "collective" failure behavior. It can be argued that no two (or more) satellites are truly alike, and that every satellite operates in a distinct environment. As a result, the situation of the space industry is very different from that for example of the semi-conductor industry where data on, say, millions of identical transistors operating under identical environmental conditions are available for statistical analysis. The consequence is that in the absence of "satellite mass production," statistical analysis of satellite failure and reliability data faces the dilemma of choosing between calculating precise "average" satellite reliability on the one hand, or deriving a possibly uncertain "specific" satellite reliability on the other hand.

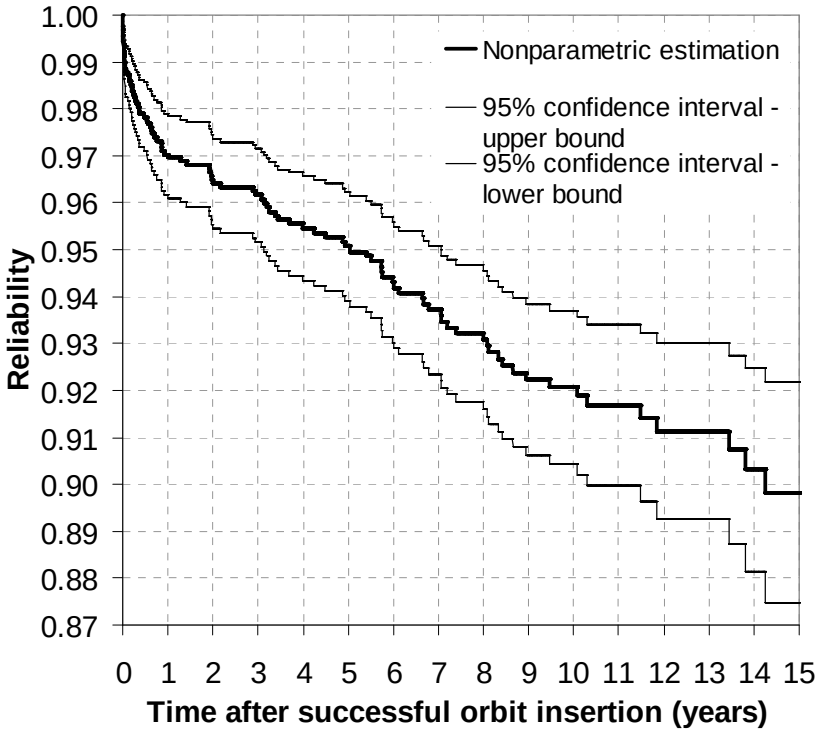

Figure 38: Satellite reliability with 95% confidence intervals [14]

This dilemma is explained in the following two possible approaches. The first approach is to lump together different satellites and analyze their "collective" on-orbit failure behavior (assuming that the failure times of the satellites are independent and identically distributed (iid)). The advantage of doing so is that one can work with a relatively large sample and thus obtain some precision and a narrow confidence interval for the "collective" reliability analyzed. The disadvantage is that the iid assumption may not be realistic, and the "collective" reliability calculated (with precision) may not reflect the specific reliability of a particular type of spacecraft. The second approach is to specialize the data, for example for specific spacecraft platform or mission type, or for satellites in particular orbits. The advantage of doing so is that the reliability analyzed is specific to the type of spacecraft considered (it is no longer a "collective" on-orbit reliability). The disadvantage is that the sample size is reduced, and as a consequence, the confidence interval expands (i.e., the results become increasingly uncertain). Given the available number of satellites (a few thousands), data specialization, which could reduce the sample size to say fewer than a hundred data points, would

result in significantly large confidence intervals, and thus highly dispersed and uncertain "specific" satellite reliability calculations.

In this study, we adopt the second approach. We discuss this approach in [15] and [16] and analyze on-orbit reliability of satellites by mission type, and mass categories (data for specific satellite platforms and by manufacturer is also available). Reliability of satellite subsystems can be found in [17].

From a statistical perspective, several parameters (covariates) or characteristics of the design can affect the probability of failure of satellites. For example, the spacecraft complexity, its orbit, the number of instruments on-board or its payload size, to name a few, have some implications on satellite reliability. One factor impacting satellite reliability might be the orbit type since the choice of orbit can impact design choices on board the spacecraft as well as the system's operating environment. Several questions follow this observation: for example, are different spacecraft orbits correlated with different failure behaviors on-orbit? Do low Earth orbit (LEO) satellites for example exhibit different failure behaviors than geosynchronous orbit (GEO) satellites? Do satellites in different orbits exhibit varying degrees of infant mortality? Etc.

For this research, we conduct statistical analysis of satellite reliability with orbit as a covariate. Our analysis is based on a data set of 1,488 Earth-orbiting satellites successfully launched between January 1990 and October 2008. We first categorize these satellites by orbit: geosynchronous orbit (GEO), low Earth orbit (LEO) and medium Earth orbit (MEO). We then conduct nonparametric analysis of satellite reliability for each orbit category using the Kaplan-Meier estimator. Using analytical techniques such as Maximum Likelihood Estimation (MLE) and least squares regression, we then conduct parametric analysis assuming 1- and 2-Weibull mixture distributions. Based on these parametric fits, we provide a comparative reliability analysis identifying similarities and differences in the reliability behaviors of satellites in these three types of orbits. Finally, beyond the statistical analysis, we conclude the second chapter of this thesis with several hypotheses for structural/causal explanations of these trends and difference in on-orbit failure behavior.

2. Database and data description

For the purpose of this study, we used the SpaceTrak® database [7]. This database provides a history of on-orbit satellite failures and anomalies, as well as launch histories since 1957 and is considered one of the most authoritative in the space industry with data for over 6,400 spacecraft. The sample we analyzed consists of 1,488 satellites. We restricted the present study to Earth-orbiting satellites successfully launched between January 1990 and October 2008. In order to compute the reliability, we used what is referred to in the database as a Class I failure, that is, a retirement of a satellite due to failure. For each spacecraft in our sample, we collect: 1) its orbit type; 2) its launch date; 3) its failure date, if failure occurred; and 4) the "censored time," if no failure occurred. This last point is further explained in the following section, where we discuss data censoring and the Kaplan–Meier estimator. The data collection template and sample data for our analysis are shown in Table 11.

Table 11: Data collection template and sample data for our statistical analysis of satellite reliability (satellites are not arranged/shown in chronological order)

Sample unit number	Orbit type	Launch date	Failure date (if failure occurred)	Censored time (if no failure occurred)
Satellite #1	GEO	11/06/1998	11/15/1998	–
Satellite #2	LEO	03/01/2002	–	10/02/2008
…		…	…	…
Satellite #1,488	MEO	04/26/2004	03/28/2006	–

The database provides information on a variety of orbits. We restricted the study to three relevant orbits: GEO, LEO, and MEO. Table 12 presents the main characteristics of the three orbit categories, and Fig. 39 provides the number of satellites per orbit category from 1990 to 2008 (i.e., the sample size for each orbit type).

Table 12: Orbit characterization

Orbit category	Characteristics
GEO	near circular with apogee and perigee at circa of 36,000km
LEO	apogee and perigee up to 2000km
MEO	near circular with apogee and perigee at circa of 20,000km

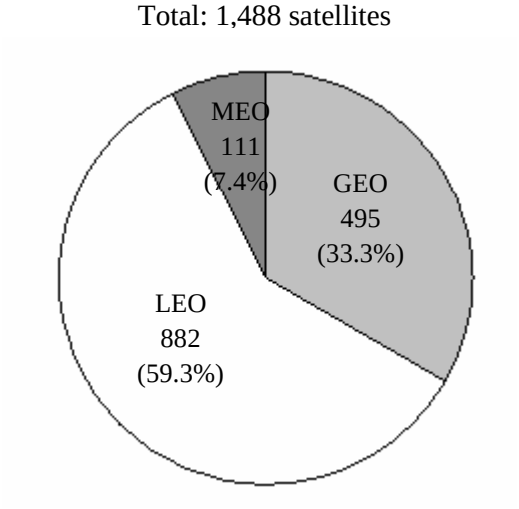

Figure 39: On-orbit satellites distribution per orbit category from 1990 to 2008

3. Non-parametric satellite reliability analysis

In this section, we briefly review censoring in statistical data analysis and the Kaplan-Meier estimator of reliability when the underlying data is right-censored, as is the case in our sample. Nonparametric means that the statistical analysis does not assume any specific parametric distribution (also referred to sometimes as distribution-free analysis). We then provide the reliability results for satellites in GEO, LEO, and MEO.

3.1. Censored Data Sample and Kaplan-Meier estimator

Censoring occurs when life data for statistical analysis of a set of items is incomplete, which is the case in our sample. More specifically, we have Type IV censoring (also known as random censoring), that is right-censoring with staggered entry. This means the following: 1) the satellites in our sample are activated at different points in time (i.e., the satellites are launched at different calendar dates) but all these activation times in our sample are known, 2) failures dates and censoring are stochastic, and 3) censoring occurs either because a satellite is retired from the sample before a failure occurs or because the satellite is still operational at the end of our observation window (October 2008). Censoring requires careful attention: deriving a reliability function from censored life data is not trivial, and it is important that it is done properly if the results are to be meaningful and unbiased. In this chapter, we adopt the Kaplan–Meier estimator [18], which is best suited for handling the type of censoring we have in our sample. The derivation of the Kaplan-Meier estimator formula can be found in [14,18]. The Kaplan-Meier estimator of the reliability function with censored data is given by Eq. (24):

$$\hat{R}(t) = \prod_{\substack{\text{all } i \text{ such} \\ \text{that } t_{(i)} \le t}} \hat{p}_i = \prod_{\substack{\text{all } i \text{ such} \\ \text{that } t_{(i)} \le t}} \frac{n_i - 1}{n_i} \tag{24}$$

where:

$t_{(i)}$: time to i^{th} failure (arranged in ascending order)

$$n_i = \text{number of operational units right before } t_{(i)}$$
$$= n - [\text{number of censored units right before } t_{(i)}]$$
$$- [\text{number of failed units right before } t_{(i)}]$$

$$\hat{p}_i = \frac{n_i - 1}{n_i} \tag{25}$$

Should there be ties in the failure times, say m_i units failing at exactly $t_{(i)}$—this situation is referred to as a tie of multiplicity m—then Eq. 25 is replaced by:

$$\hat{p}_i = \frac{n_i - m_i}{n_i} \tag{26}$$

If a censoring time is exactly equal to a failure time, a convention is adopted that assumes censoring has occurred immediately after the failure (that is, at an infinitely small time interval after the failure).

3.2. Non-parametric reliability results of GEO, LEO, and MEO satellites

With this brief overview of censoring and the Kaplan-Meier estimator, we can now analyze the on-orbit satellite reliability from our censored data sets. For the 1,488 satellites analyzed, and the 3 orbit categories here considered, we obtained 22 Class I failures for the GEO category, 70 for the LEO category, and 2 for the MEO category. The data was then treated with the Kaplan-Meier estimator (Eq. 24), and we obtained the non-parametric reliability results of GEO, LEO, and MEO satellites shown in Fig. 40 and 41.

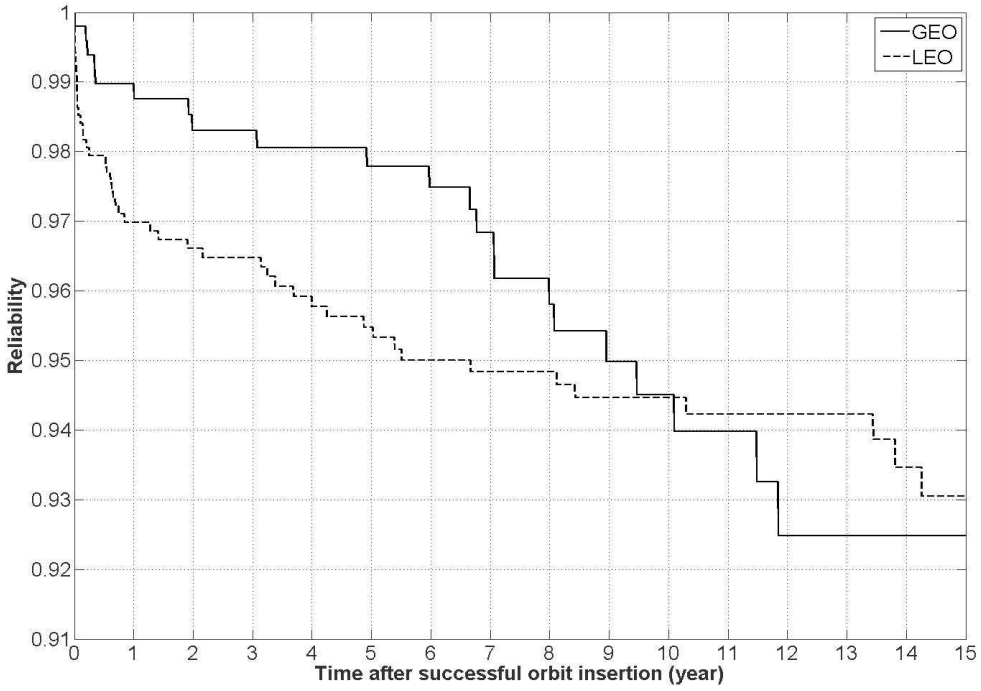

Figure 40: Nonparametric results of GEO and LEO satellites reliability

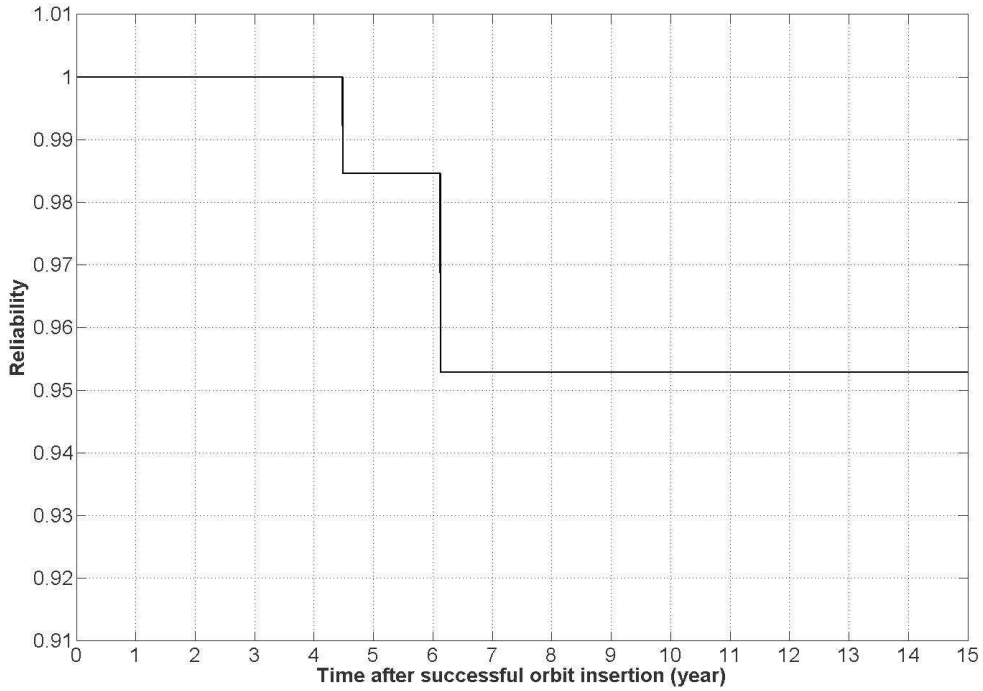

Figure 41: Nonparametric result of MEO satellites reliability

Figure 40 and 41 are known as the Kaplan plots of reliability. Vertical cuts across Fig. 40 read as follows, for example:

- The most likely estimate of GEO satellites reliability at t = 1 year on-orbit is $\hat{R}$ = 98.7%.

- The most likely estimate of GEO satellites reliability at t = 7 year on-orbit is $\hat{R}$ = 96.8%.

The Kaplan plots for the GEO, LEO, and MEO satellites allow us to visually identify some important trends in satellite reliability and on-orbit failure behavior. For example:

1. GEO satellites exhibit a small infant mortality, with a reliability dropping to approximately 98.7% after one year. In addition, GEO satellites exhibit a clear wear-out failure behavior between 6 and 12 years, with a reliability dropping from 97.5% to 92.5% (Fig. 40).

2. LEO satellites exhibit a significant infant mortality, with a reliability dropping to 97% after one year. In addition, between the third and the sixth year, a “light” wear-out failure behavior can be observed with a reliability dropping from approximately 96.5% to 95% (Fig. 40).

3. For the MEO satellites (Fig. 41), only two failures can be observed over 111 MEO satellites. As a result, no significant conclusions can be drawn about the nonparametric reliability results of these satellites.

These trends will be explored more closely and analytically in Sections 4 and 5.

4. Parametric reliability analysis

Nonparametric analysis provides important results since the reliability calculation is not constrained to fit any particular pre-defined lifetime distribution. However, this flexibility makes nonparametric results neither easy nor convenient to use for various purposes often encountered in engineering design (e.g., reliability-based design optimization). In addition, some failure trends and patterns are more clearly identified and recognizable with parametric analysis. Several possible methods are available to fit a parametric distribution to the nonparametric reliability function (as provided by the Kaplan-Meier estimator). In the following, we present two parametric methods based on the Weibull distribution to fit the nonparametric reliability of satellites in each orbit category discussed previously.

4.1. Weibull distribution

The Weibull distribution is one of the most commonly used distribution in reliability analysis. Its reliability (or survivor) function can be written as follows:

$$R(t) = \exp\left[-\left(\frac{t}{\theta}\right)^{\beta}\right] \qquad \text{for } t \geq 0 \tag{27}$$

where β is the shape parameter (dimensionless) and θ the scale parameter (units of time), both nonnegative. The reason for the wide adoption of the Weibull distribution is that it is quite flexible, and with an appropriate choice of the shape parameter β, it can capture different kinds of failure behaviors. For example, when $0 < \beta < 1$, the Weibull distribution models infant mortality (which corresponds to a decreasing failure rate); when $\beta = 1$, the Weibull distribution becomes equivalent to the Exponential distribution (constant failure rate); and when $\beta > 1$, the Weibull distribution models wear-out failures (which corresponds to an increasing failure rate).

In previous publications, we demonstrated the appropriateness of the Weibull distribution as a parametric model for satellite reliability [14,17,19]. In this section, we first derive Weibull fits for the three nonparametric reliability results using the Maximum Likelihood (MLE) procedure. However, the parametric results will be shown to be within 0.6 to 3.2 percentage points of the "benchmark" nonparametric results, and for our purposes, these results are not sufficiently accurate. We therefore proceed with deriving mixture Weibull distributions for the nonparametric results and demonstrate a significant improvement in the accuracy of the parametric fits. The details are discussed next.

4.2. Maximum Likelihood Estimation (MLE) of single Weibull fit

Details of the Maximum Likelihood Estimation procedure can be found in [20], and its analytic derivation is provided in [17]. When applied to the nonparametric reliability results shown in Fig. 40 and 41, the MLE procedure yields the Weibull parameter estimates for each satellite orbit category. The results are provided in Table 13.

Table 13: Maximum Likelihood Estimates of the Weibull parameters for satellite reliability across the three orbit categories

Orbit category	β	θ
		years
GEO	0.7190	582.5
LEO	0.3473	34048.9
MEO	1.6347	79.4

The information in Table 13 reads as follows. Consider for example the GEO satellites. Its nonparametric reliability is best approximated by the following MLE-derived Weibull distribution:

$$R_{GEO}(t) = \exp\left[-\left(\frac{t}{582.5}\right)^{0.719}\right] \tag{28}$$

The values of the shape parameter (β = 0.7190) and the scale parameter (θ = 582.5) are the Maximum Likelihood Estimates. Figure 42 shows the nonparametric reliability curve and the MLE-derived Weibull fit for the three orbit categories.

For satellites in LEO, Fig. 42 provides a visual verification that the MLE-derived Weibull distribution is a satisfying fit for the nonparametric reliability. It is difficult to derive the same conclusion for the two other orbit categories.

The goodness-of-fit of the Weibull distribution is reflected in this section by the maximum and average errors over 15 years between the nonparametric reliability results (the "benchmark" results) and the Weibull fit. Table 14 provides the maximum and average error between the nonparametric reliability and the Weibull fit for the three orbit categories. Despite this reasonable accuracy of the

parametric fit, Fig. 42 shows that the single Weibull distribution does not fully capture the failure trends in the data, especially for the GEO and MEO satellites. To improve the quality of the parametric fit, we derive in the next subsection mixture Weibull distributions for the non-parametric reliability results derived in Section 3.

Table 14: Error between the nonparametric reliability and MLE Weibull fit for each satellite category

Orbit category	**Maximum error** (percentage point)	**Average error** (percentage point)
GEO	1.6	0.7
LEO	0.6	0.2
MEO	3.2	1.0

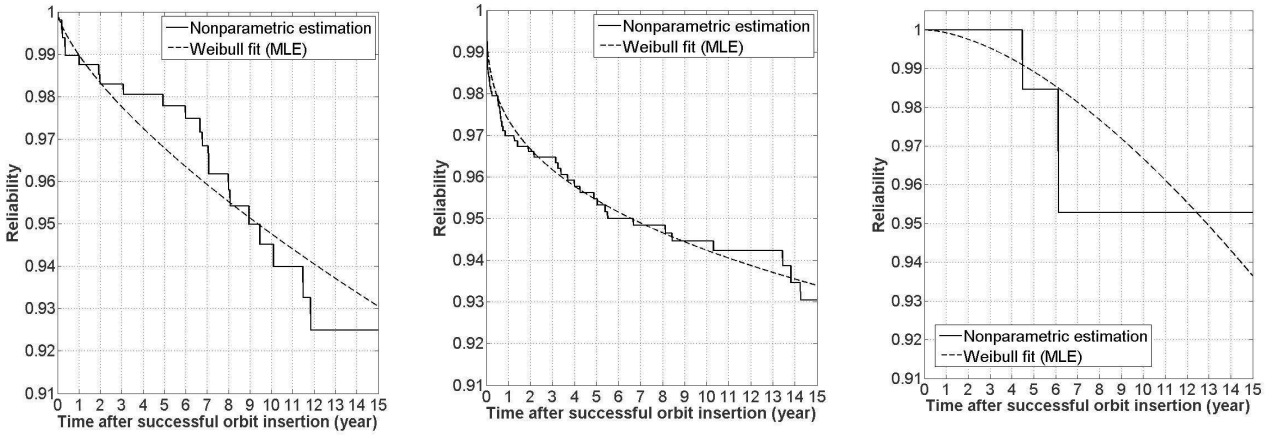

GEO category LEO category MEO category

Figure 42: Nonparametric reliability and single Weibull fit

4.3. Mixture distributions

Several distributions such as the Exponential, Weibull, or Lognormal, can be used as a basis for linear combination to generate a mixture distribution. In this subsection, we maintain the Weibull as the basis for our parametric calculations and derive mixture of two Weibull distributions for the nonparametric satellite reliability of each orbit category. The parametric reliability model with a mixture of two Weibull distributions can be expressed as follows:

$$R(t) = \alpha \exp\left[-\left(\frac{t}{\theta_1}\right)^{\beta_1}\right] + (1-\alpha)\exp\left[-\left(\frac{t}{\theta_2}\right)^{\beta_2}\right] \tag{29}$$

The parameter α is used to modify the relative weight given to each Weibull distribution in the mixture. A generalized expression for *n* mixture distributions is provided in [21]. We restrict our calculations in this section to $n = 2$ since as will be shown shortly, the results are significantly accurate and the 2-Weibull distributions follows with notable precision the different failure trends in the nonparametric results. Limited incremental accuracy is provided by 3-Weibull mixture distributions. Increasing *n* provides insignificant accuracy improvement.

The nonlinear least squares method provides us with the best fits for the parameters of the 2-Weibull mixture distribution for each orbit category. The results are provided in Table 15. For the three orbit categories, the new parametric fit of the reliability using a 2-Weibull mixture distribution accurately follows the nonparametric reliability, as shown in Fig. 43.

It is worth pointing out that the first Weibull element with a shape parameter $\beta_1 < 1$ captures satellite infant mortality while the second Weibull element with a shape parameter $\beta_2 > 1$ captures satellite wear-out failures. As expected, the fits provided by the mixture distributions approach for the three orbits categories are better than those provided by the MLE approach. Table 16 provides the R^2 coefficients and the sum of the squares of errors (SSE) of the three mixture distributions formulated for each orbit category. The R^2 coefficients of the fits are higher than 97% for the three categories. To gauge the precision improvement between the single Weibull and the 2-Weibull

mixture distributions, we calculate both the maximum and the average error between the nonparametric reliability (the benchmark results) and the parametric models. The results are shown in Table 17.

Table 15: 2-Weibull mixture distribution parameters

Orbit category	α	β_1	β_2	θ_1	θ_2
					years
GEO	0.0496	4.1070	0.3300	9.8	661600.0
LEO	0.9927	0.2997	68.6300	136100.0	14.4
MEO	0.9526	1.4790	8.3600	101900.0	6.0

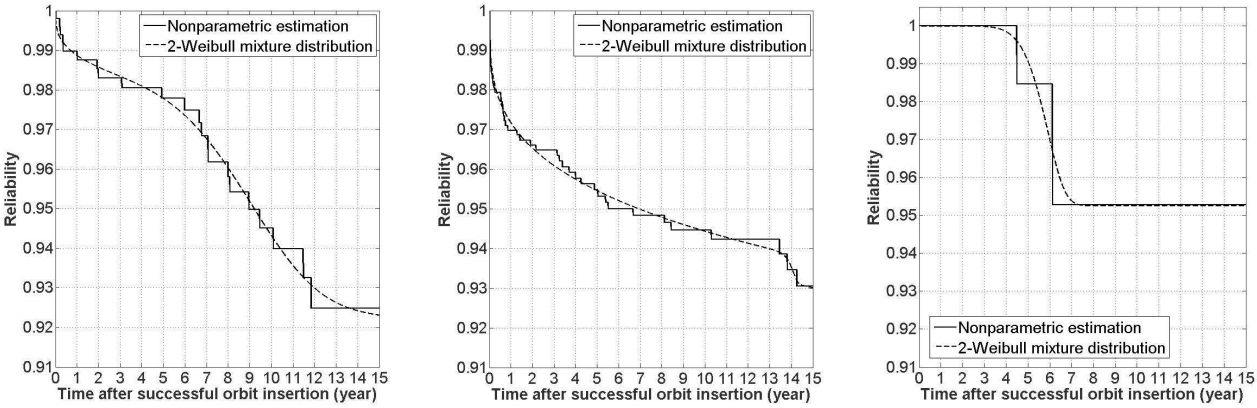

GEO category LEO category MEO category

Figure 43: Nonparametric reliability and 2-Weibull mixture fit for the three satellite categories

Table 16: Goodness-of-fit of the 2-Weibull mixture distribution for each satellite category

Ceofficient	Orbit category		
	GEO	**LEO**	**MEO**
R^2	0.9908	0.9845	0.9749
SSE	0.03978	0.01698	0.08776

Table 17: Error between the nonparametric reliability and the parametric models over 15 years

Orbit category	Error	Parametric fit	
	percentage point	Single Weibull	2-Weibull mixture
GEO	maximum error	1.6	0.7
	average error	0.7	0.2
LEO	maximum error	0.6	0.4
	average error	0.2	0.1
MEO	maximum error	3.2	1.8
	average error	1.0	0.2

As seen in Table 17, the 2–Weibull mixture distribution is significantly more accurate than the single Weibull distribution in capturing the (benchmark) nonparametric satellite reliability. Section 3 briefly presented the general trends in the nonparametric reliability curves of each orbit category. In order to lead further investigations on the behavioral differences between the three satellite categories, the next section provides a detailed comparative analysis of the satellite reliability across orbit categories based on the mixture distributions previously developed.

5. Comparative analysis of satellite reliability across orbit categories

In this section, we revisit our findings regarding the difference in the reliability results of satellites in different orbit categories. Figure 44 shows the failure rates (or hazard function) of the GEO and LEO orbit categories. Due to a limited number of failures, the failure rate of the MEO orbit category is thought to be insignificant and will not be discussed here. The y-axis is provided in log-scale for readability purpose. The left panel in Fig. 44 provides a closer look at the failure rate over the short time periods (through the use of a log-scale on the x-axis).

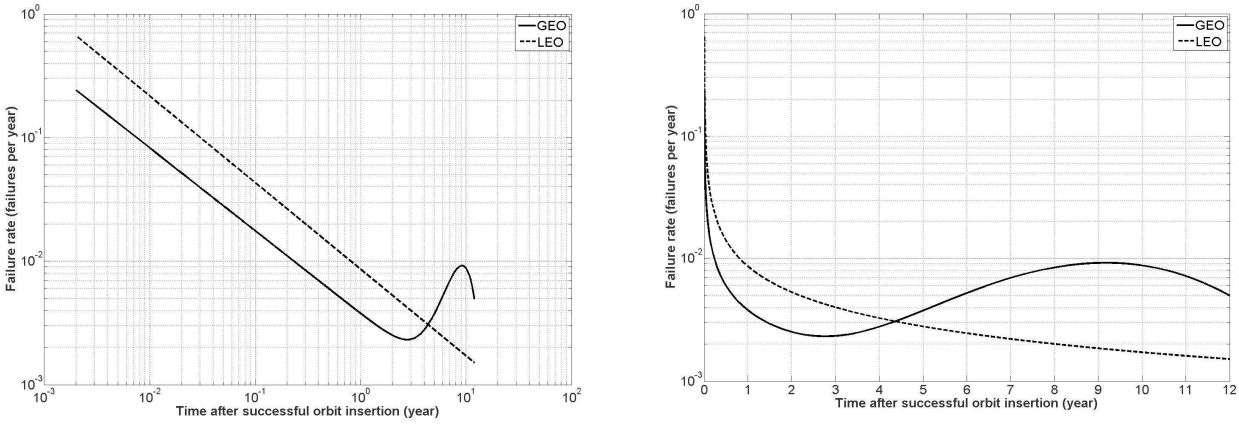

Figure 44: Failure rates of GEO and LEO satellite categories

The failure rate *R(t)* uniquely determines the reliability function through Equation 30:

$$R(t) = e^{-\int_0^t \lambda(t')dt'} \tag{30}$$

First, we can notice on Fig. 44 that the failure rate of the LEO orbit category is significantly higher during the first 4 years after successful orbit insertion than for the GEO orbit category. It confirms the infant mortality behavior of the LEO category highlighted in the previous section. In addition, we observe an important increase of the GEO category failure rate between 6 and 12 years. During this period of time, the failure rate of the GEO category clearly exceeds the failure rate of the LEO category, which reflects a previous result that GEO satellites exhibit a wear-out behavior between 6 and 12 years after orbit insertion.

Next, we identify periods of time during which the reliability of the orbit categories show similarities or differences in their behavior. Figures 45 and 46 present the absolute difference in satellite reliability for each pair of orbit categories: LEO/MEO, LEO/GEO, and MEO/GEO. More than characterizing the amplitude of the difference itself, we ultimately seek to identify a period of time during which the difference remains approximately constant, meaning that the two reliability curves have the same behavior. For example, a significant increase of the absolute difference early in time after successful orbit insertion during $[0, t_1]$, followed by a relatively constant evolution of the difference during $[t_1, t_2]$, would mean that the two reliability curves do not exhibit similar infant mortality behavior during $[0, t_1]$ but also that they do show similar behavior later in time during $[t_1, t_2]$. First we can notice that all the three differences jump up to 1 percentage point during the first year following orbit insertion. This result indicates that satellites across the three orbit categories have different failure behavior early on orbit, that is they have different infant mortality behavior. A quick glance at Fig. 45 and Fig. 46 also reveals that significant periods of time during which any of the three reliability differences remains roughly constant are difficult to find. The only period of interest would eventually be between 3 and 6 years for the LEO/GEO difference (Fig. 45) but yet, the periods responsible for similarities and differences between reliability profiles are not explicitly identified.

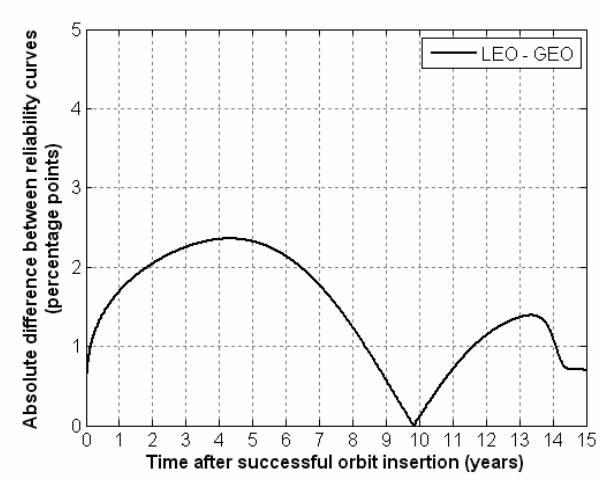

Figure 45: LEO/GEO reliability difference in satellite reliability over time

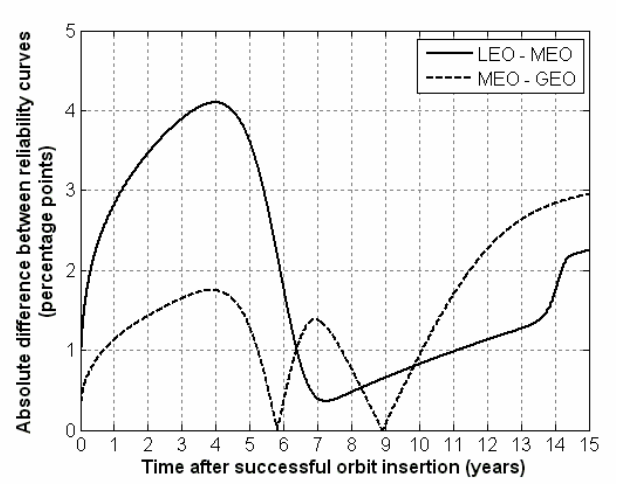

Figure 46: LEO/MEO and MEO/GEO reliability differences in satellite reliability over time

To better assess whether the reliability and failure behavior of two different orbit categories are similar after a given period, we investigate their conditional reliabilities. For an item that has survived until time *T*, the conditional reliability allows the calculation of its probability of survival for an additional period of operation, knowing that the item has survived until *T*. By considering conditional reliabilities, we can perform a comparative analysis of failure behavior of the different satellite categories over different time periods and by selectively filtering out or disregarding failures prior to *T*. The benefits of doing so will be demonstrated shortly. Using the time domains shown in Fig. 47, the conditional reliability is defined as follows [22,23]:

$$R(t|T) = \Pr\{T_F > T + t | T_F > T\} \tag{31}$$

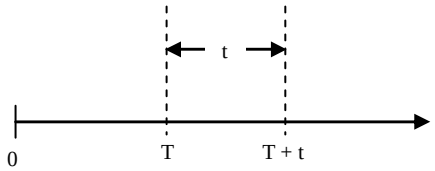

Figure 47: Time domains for conditional reliability from [23]

T_F is the random variable Time-to-Failure. By definition of the conditional probability and the reliability function, (Eq. 31) can be reduced to:

$$R(t|T) = \frac{\Pr\{T_F > T + t\}}{\Pr\{T_F > T\}} = \frac{R(T+t)}{R(T)} \tag{32}$$

The conditional reliability is particularly useful for the study of a burn-in and its impact. In our case, we make a related, although broader, use of conditional reliabilities to study the failure behavior of satellites in different orbit categories. The conditional reliability is useful for comparing two different reliability curves. Indeed, the conditional reliability "eliminates" or filters out the failure behavior of the system up to the time T. To illustrate the relevance of this observation for our study purposes, consider the following two systems, the first one suffering from significant infant mortality during the [0; t_1] period, and the second one is not. In addition, the two systems have the same failure behavior during the [t_1; t_2] period. The reliability curves of these two systems will be different and hardly comparable. While the reliability curves will clearly indicate the difference in infant mortality behavior between the two systems, these curves will not identify the similarity in failure behavior between the two systems during the [t_1; t_2] period. The difference between the curves is only due to the failures during the initial [0; t_1] period. Thus, by setting $T = t_1$, in Eq. 32, we can calculate the two conditional reliability curves over [t_1; t_2], and the two resulting curves will be similar, due to the same failure behavior during this period. By filtering out the failures during the initial period, the similarity of the failure behavior of the two systems during [t_1; t_2] can thus be clearly identified. Hence, by carefully selecting the appropriate time(s) T, the conditional reliability helps us separate the impact of early failures, and clearly determine periods of similar failure behavior, if they exist.

Guided by visual inspection of Figure 45, we iteratively examined various evaluation times T. The most significant and meaningful cases are discussed next. For the LEO and GEO categories, we suggested that the absolute difference remains roughly constant (varying by less than 0.2 percentage point) between 3 and 6 years after orbit insertion, which might demonstrate a similar reliability behavior during this time period. Figure 48 shows the absolute difference between the conditional reliabilities for satellites that have survived 3 years, that is for T = 3 years, for the LEO and GEO categories. As the figure shows, no reliability data is shown until $t = T$. Until t = 6 years, the absolute difference between the conditional reliabilities varies very little and remains below 0.2

percentage points. After t = 6 years, the absolute difference between the conditional reliabilities increases significantly, suggesting a divergence of the two failure behaviors of satellites in LEO and GEO. This phenomenon can be verified in Fig. 49, which shows the conditional reliabilities evaluated for T = 3 years for the GEO and LEO satellites. The two reliability curves are almost overlapping between 3 and 6 years, then a significant divergence occurs between the two curves after t = 6 years.

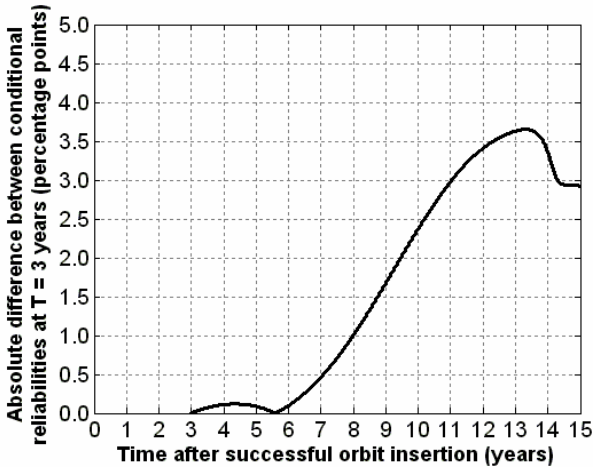

Figure 48: Absolute difference in conditional reliability evaluated for T = 3 years between GEO and LEO satellites

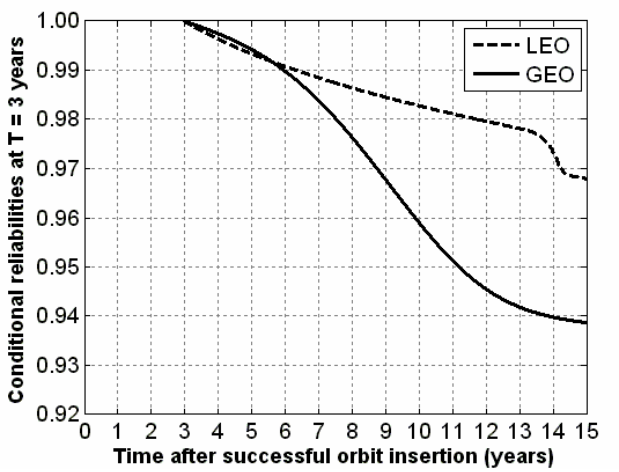

Figure 49: Conditional reliabilities evaluated for T = 3 years between GEO and LEO satellites

Regarding the other comparative reliability analyses, namely between LEO/MEO and GEO/MEO, no significant period of time was found showing similar failure behavior. In addition, the small sample size of the MEO satellites (111 satellites) and only 2 failures renders it difficult to make strong inferences about the actual reliability and on-orbit failure behaviors of these satellites (more details on this point can be found in the appendix).

In the next section, we discuss several hypotheses for possible structural/causal explanations of the difference in reliability and failure behavior of satellites across orbit categories.

6. Hypothesis for causality analysis

The previous sections demonstrated that there are significant differences in the reliability and failure behavior of the LEO and GEO satellites. This section explores possible causes of these differences. The most obvious factor that varies from one orbit category to another is the space environment. The space operating environment strongly influences the performance and lifetime of on-orbit satellites and can lead to costly malfunctions or loss of subsystems and spacecraft [24]. The space environment, as a function of orbit choice, also impacts design decisions and has implications on satellite size, weight, complexity, and cost [25], all of which can impact satellite reliability. Programmatic considerations can also be important influencing factors of satellite reliability. These hypotheses are discussed next.

6.1. Environmental Factors

6.1.1. Upper Atmosphere

One obvious difference between LEO and the higher MEO and GEO orbits is the rarefied atmosphere present in LEO. This results in aerodynamic drag that must be counteracted for a satellite to remain in orbit for long periods of time. Orbit lifetime for typical satellites is on the order of a few months at 300 km altitude and a few years at 400 km altitude [26]. However, orbit lifetime estimates are subject to significant uncertainty because they are limited by the accuracy of drag and space weather models [27]. Two well-known examples of unintended re-entries due to inadequate drag predictions are the American Skylab and Soviet Salyut 7 space stations. Skylab was originally expected to remain in orbit ten years after the last crew departed in 1974, allowing for potential servicing by the Space Shuttle. However, Skylab became the victim of unexpectedly high solar activity and re-entered in 1979 [28]. Similarly, it was intended for Salyut 7 to remain in orbit 8-20 years after its 1986 decommissioning for potential retrieval by the Soviet *Buran* space shuttle. However, it re-entered in February 1991 due to unexpected solar activity which raised upper atmospheric density by factors of 4-5. Furthermore, a local peak in solar activity in late January

1991 prevented the impact location from being known more accurately than within a half-orbit until just three hours prior to impact [27, 29].

Since atmospheric drag effects and their associated uncertainties typically manifest themselves gradually, they are rarely the direct causes of satellite failures. However, they do affect decommissioning dates for LEO satellites and may exacerbate the effects of otherwise more minor failures. For example, upper atmosphere drag on LEO satellites may result in shorter windows during which an operations team can effectively recover the satellite from propulsion, attitude control, or communications failures before drag losses or drag-induced torquing effects become too large.

In addition, the upper atmosphere is associated with chemically corrosive effects of highly reactive species such atomic oxygen. This form of oxygen, predominant from about 200 km to 600 km in altitude, can react with organic films, composite materials, and metallized surfaces, causing degradation on sensor performance [30]. Solar arrays and space mirrors are an example of subsystems that encounter a degradation problem caused by the impact of atomic oxygen in the LEO environment [24, 31]. Extensive erosion due to atomic oxygen is one failure mechanism in LEO that does not exist in the GEO and MEO orbits.

6.1.2. Plasma and Magnetic Field

Ionization of the space environment is highly dependent on altitude. At about 300 km, 1% of the atmosphere is ionized while this number increases to 100% ionization in the geosynchronous environment. These charged particles, forming the plasma environment, charge the surface of any spacecraft within it to high negative voltages. If the local electric field exceeds the breakdown field along the surface of the material, it can trigger an electrostatic arc and electromagnetic interference (EMI) large enough to disrupt electronic components [32]. This has been attributed as a major failure mode for GEO satellites, particularly as they emerge from an eclipse period into a solar storm [33]. At low altitude, this charged phenomenon only appears in the high latitudes regions,

where auroral electrons collide with the spacecraft. It is yet much more common for higher orbits, such as GEO.

6.1.3. Radiation

There are several types of radiation that may threaten Earth-orbiting spacecraft. Since these types of radiation impact satellites in distinct altitude ranges, they are also candidate explanations for differences in reliability behavior among LEO, MEO, and GEO satellites.

- The Van Allen radiation belts consist of electrons and ions with energies greater than 30 keV. They are distributed nonuniformly within the magnetosphere up to a distance of 7 Earth radii. It is usually acknowledged that space missions beyond low Earth orbit leave the protection of the geomagnetic field, and transit the Van Allen belts. Thus they face more threats caused by the Van Allen radiations. The region between two to three Earth radii lies between the two radiation belts and is sometimes referred to as the “safe zone” [34].

- Solar particle events (SPEs) occur in association with solar flares. They are rapid increases in the flux of energetic particles, from 1 MeV to above 1 GeV, and can last from several hours to several days. Ultimately, they can lead to degradation of solar arrays or electro-optical sensors [25]. Depending on their energy level, the SPEs penetrate the Earth magnetosphere at different altitudes. It is more likely that they will impact high altitude orbits, such as geosynchronous orbits, than low-Earth orbits.

6.2. Thermal and Power Cycling

In addition to space environment effects, another substantial difference among the three orbit categories is the degree of thermal and power cycling. In a one-day period, a 400 km LEO satellite orbits the Earth about sixteen times, while a GEO satellite orbits the Earth once. As a result, the LEO satellite cycles between eclipse and sunlight periods at least sixteen times as often as the GEO satellite, subjecting the LEO satellite to substantially more thermal and power cycling. It is

reasonable to consider that thermal expansion and contraction effects could cause component fatigue, particularly for delicate components. It is also plausible that power subsystem cycling, especially for the battery's charge and discharge in and out of eclipse, could cause different failure modes for satellites in LEO and GEO. Cycling effects may be one contributor to the substantial infant mortality exhibited in the LEO satellite reliability data.

6.3. Programmatic Effects

A final hypothesis for differences in the observed LEO and GEO satellite reliability behavior deals with the effect of programmatic decisions. Typically, GEO satellites are designed for use over a period of time on the order of a decade or more. In contrast, LEO satellite design lifetimes are generally shorter, often less than five years. The development of potentially more expensive and longer-lived GEO satellites is likely to include more investment in quality control testing, and more focus on reliability, part selection, and redundancy. The much lower infant mortality for GEO satellites may be attributable to this system development consideration.

7. Conclusion

We derived in this chapter nonparametric and parametric reliability results for Earth-orbiting satellites as a function of orbit type, namely geosynchronous orbits (GEO), low Earth orbits (LEO) and medium Earth orbits (MEO). We used an extensive database of satellite launches and on-orbit failures and anomalies to derive, using the Kaplan-Meier estimator, nonparametric reliability results for each satellite category. Next, using the Maximum Likelihood Estimation (MLE) technique and least squares regression, we derived parametric fits of the results with single and 2-Weibull mixture distributions. The parametric fits using the mixture distributions proved to be significantly accurate in capturing the failure trends in the nonparametric results. Based on these parametric fits, we provided a comparative reliability analysis identifying similarities and differences in the reliability behaviors of satellites in these three types of orbits. Finally, beyond the statistical analysis, we concluded this second chapter of the thesis with several hypotheses for structural/causal explanations of these trends and difference in on-orbit failure behavior.

Appendix: Confidence interval analysis

The Kaplan-Meier estimator (Eq. 24) provides a maximum likelihood estimate of reliability but does not inform us about the dispersion around $\hat{R}(t_i)$. This dispersion is captured by the variance or standard deviation of the estimator, which is then used to derive the upper and lower bounds for a 95% confidence interval (that is, a 95% likelihood that the actual reliability will fall between the two calculated bounds, with the Kaplan-Meier analysis providing us with the most likely estimate). The variance of the estimator is provided by Greenwood's formula (Eq. 33), and the 95% confidence interval is determined by Eq. 34.

$$\hat{\text{var}}[R(t_i)] \equiv \sigma^2(t_i) = \left[\hat{R}(t_i)\right]^2 \cdot \sum_{j \le i} \frac{m_j}{n_j(n_j - m_j)} \tag{33}$$

$$R_{95\%}(t_i) = \hat{R}(t_i) \pm 1.96 \cdot \sigma(t_i) \tag{34}$$

More details about these equations can be found in [35, 36, 37].

When Eqs. (33) and (34) are applied to the data within each category along with the Kaplan-Meier estimated satellite reliability $\hat{R}(t_i)$ shown in Fig. 40 and 41, we obtain the 95% confidence interval curves. These results for each orbit category of satellites are shown in Fig. 50. It shows for example that the GEO Satellites reliability at t = 1 year will be between 97.7% and 99.7% with a 95% likelihood—these values constitute the lower and upper bounds of the 95% confidence interval at t = 1 year. Notice that the dispersion of $R(t_i)$ around $\hat{R}(t_i)$ increases with time. This increase in dispersion can be seen in Fig. 50 by the growing gap between the Kaplan–Meier estimated reliability and the confidence interval curves. This phenomenon illustrates the increasing uncertainty or loss of accuracy of the statistical analysis of satellite reliability with time resulting from the decreasing sample size.

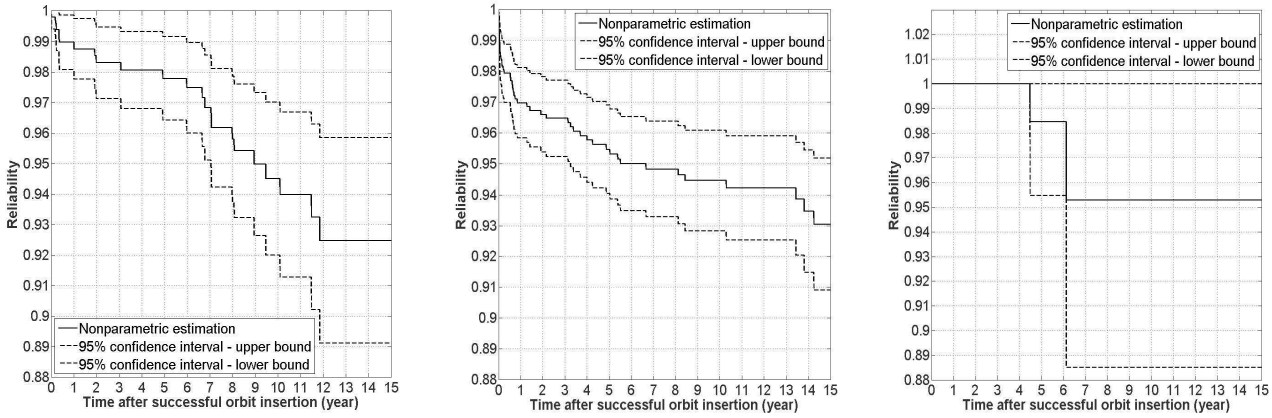

GEO category LEO category MEO category

Figure 50: Satellite reliability with 95% confidence intervals for each orbit category

CONCLUSION

In the work accomplished for this Master thesis, we brought statistical analysis techniques to bear on data derived from an extensive database of satellite launches, on-orbit anomalies and failures, and conducted two separate studies addressing distinct research objectives.

In the first study, we analyzed time series of satellite launches between 1960 and 2008. We identified trends and fluctuations, and clearly demonstrated the existence of cycles in satellite launch volume. Cyclicality was empirically shown across three satellite categories (and consequently three satellite *markets*): 1) Defense and Intelligence (D&I) satellites, 2) Science satellites, and 3) Communication satellites. In addition, the cycles were identified over two time periods: the entire data window (1960 to 2008), and over roughly the last decade. Distinct cycles of 3.1 years exist in launch volume for the D&I and Science satellites. The situation is a little bit more ambiguous for the communication satellites primarily because of the structural anomaly in the data for this satellite category, due to the Low Earth Orbit communication satellites "bubble" and its burst between 1996 and 2000. It is not yet clear how this market will evolve or settle.

A possible extension of the work herein lies in the application of Wavelet theory to the time series introduced in this thesis. As illustrated in this thesis, the Fourier transform provides the frequency-amplitude representation of the signal of interest and demonstrates how much of each frequency exists in that signal. Yet, it does not provide any information regarding the time of occurrence of these frequency components. The Wavelet transformation, unlike the Fourier transform, is capable of providing the time and frequency information simultaneously, hence giving a time-frequency representation of the signal. Having the time localization of the spectral components present in the time series should allow correlating the cyclical behaviors found in the data with some particular periods of time. Then, based on the Fourier and Wavelet analyses, future work could also consist of developing hypothesis and theories in order to explain the cyclical behaviors highlighted in this thesis, as well as their temporal appearances. For example, it might be interesting to try to correlate temporal appearances of launch volume's cyclical components with new launchers development, with government's changes or with significant modifications of the economical and geopolitical

environment. Finally, it would also be interesting to conduct a similar study by analyzing time-series of the data specialized by orbit, satellite manufacturers, or per launchers.

In the second statistical study, we derived nonparametric and parametric reliability results for Earth-orbiting satellites as a function of orbit type, namely geosynchronous orbits (GEO), low Earth orbits (LEO) and medium Earth orbits (MEO). We used an extensive database of satellite launches and on-orbit failures and anomalies to derive, using the Kaplan-Meier estimator, nonparametric reliability results for each satellite category. Next, using the Maximum Likelihood Estimation (MLE) technique and least squares regression, we derived parametric fits of the results with single and 2-Weibull mixture distributions. The parametric fits using the mixture distributions proved to be significantly accurate in capturing the failure trends in the nonparametric results. Based on these parametric fits, we provided a comparative reliability analysis identifying similarities and differences in the reliability behaviors of satellites in these three types of orbits. Finally, beyond the statistical analysis, we concluded the second part of the thesis with several hypotheses for structural/causal explanations of these trends and difference in on-orbit failure behavior.

One of the limitations of such a reliability analysis concerns the binary characterization of the state of the satellite, either operational or failed. By introducing “degraded states” or partial failures, a multi-state failure analysis would provide additional information regarding the degradation behavior of an item over time, until total failure occurs. Much insight could be gained by considering the frequency of occurrence of each type of failure.
Moreover, in addition to the data specialization by orbit, the analysis of spacecraft reliability by subsystems would help understand better the structural reasons of satellite failures and would furthermore offer opportunities to formulate new strategies to prevent such failures. At the mission design level, such analyses would pave the ground for the formulation of new reliability models that could be used to predict (and compare) the reliability of different space architectures.

We hope that these two studies will provide helpful feedback to the space industry regarding the cyclicality in the space industry and the on-orbit failure behavior of satellites, and that it will invite other contributors to explore some of the issues raised in this Master thesis.

REFERENCES

[1] Schumpeter, J. A., “History of Economic Analysis”, Oxford University Press, New York, NJ, 1954.

[2] Sullivan, A., Sheffrin, S. M., “Economics: Principles in Action”, Prentice Hall, Upper Saddle River, NJ, 2003.

[3] Barro, R. J., “Modern Business Cycle Theory”, Harvard University Press, Cambridge, MA, 1989.

[4] Achinstein, A., “Introduction to Business Cycles”, Crowell, New York, NJ, 1950.

[5] Noam, E. M., “Fundamental Instability: Why Telecom is Becoming a Cyclical and Oligopolistic Industry”, Information Economics and Policy, Vol. 18, No. 3, 2006, pp. 272-284.

[6] Morgan, M. S., “The History of Econometric Ideas”, Cambridge University Press, Cambridge, MA, 1991.

[7] Ascend SpaceTrak® database, online database. [http://www.ascendworldwide.com/spacetrak.aspx.]

[8] Bracewell R.N., “The Fourier Transform and Its Applications”, McGraw-Hill, New York, NJ, 1965.

[9] Walker, J. S., “Fast Fourier Transforms”, CRC Press, Boca Raton, FL, 1996.

[10] Donnelly, D., Rust B., “The Fast Fourier Transform for Experimentalists, Part I: Concepts”, Computing in Science & Engineering, Vol. 7, No. 2, 2005, pp. 80-88.

[11] Castet, J.-F., Saleh, J. H., “Satellite Reliability: Statistical Data Analysis and Modeling”, Journal of Spacecraft and Rockets, Vol. 46, No. 5, 2009.

[12] Thode, H. C., “Testing for Normality”, Marcel Dekker, New York, NJ, 2002.

[13] Filliben, J. J., “The Probability Plot Correlation Coefficient Test for Normality”, Technometrics, Vol. 17, No. 1, 1975, pp. 111-117.

[14] Castet, J.-F., Saleh, J. H., “Satellite Reliability: Statistical Data Analysis and Modeling”, Journal of Spacecraft and Rockets, Vol. 46, No. 5, Sept/Oct 2009.

[15] Castet, J-F., Saleh, J. H., “Geosynchronous Communication Satellite Reliability: Statistical Data Analysis and Modeling”, 27th AIAA International Communications Satellite Systems Conference (ICSSC 2009), Edinburgh, Scotland, 1-4 June 2009.

[16] Dubos, G. F., Castet, J-F., Saleh, J. H., “Statistical Analysis of Satellite Reliability Specialized by Mass Categories: Does (Spacecraft) Size Matter?”, 60th International Astronautical Congress, Daejeon, Republic of Korea, 12-16 October 2009.

[17] Castet, J-F., Saleh, J. H., “Satellite and Satellite Subsystems Reliability: Statistical Data Analysis and Modeling”, Reliability Engineering and System Safety, Vol. 94, No. 11, pp. 1718-1728, Nov. 2009.

[18] Kaplan, E. L., Meier, P., “Nonparametric Estimation from Incomplete Observations”, Journal of the American Statistical Association 1958; 53(282): 457-481.

[19] Castet, J-F., Saleh, J. H., “Modeling for Nonparametric Satellite Reliability: Graphical Versus Maximum Likelihood Estimations”, submitted to Journal of Spacecraft and Rockets, April 2009.

[20] Lawless, J. F., “Statistical models and methods for lifetime data”, 2nd ed., New York: John Wiley & Sons, 2003.

[21] Castet, J-F., Saleh, J. H., “Single versus mixture Weibull distributions for nonparametric satellite reliability”, submitted to Reliability Engineering and System Safety, May 2009.

[22] Ebeling, C. E., “An Introduction to Reliability and Maintainability Engineering”, New York: McGraw-Hill, 1996.

[23] Kececioglu, D., “Reliability Engineering Handbook”, Englewood Cliffs, N.J. : Prentice-Hall, 1991.

[24] Hastings, D., Garrett, H., “Spacecraft-Environment Interactions”, New York: Cambridge University Press, 1996.

[25] Tribble, A. C., “The Space Environment and Survivability”, in: Wertz, J. R., Larson, W. J., Space Mission Analysis and Design, Space Technology Library, 1999.

[26] Larson, W.J., and Wertz, J.R. (ed.), “Space Mission Analysis and Design”, 3rd ed., Microcosm Press and Kluwer Academic Publishers, El Segundo, 1999.

[27] Doornbos, E. and Klinkrad, H., “Modelling of space weather effects on satellite drag”, Advances in Space Research, Vol. 37, No. 6, 2006. pp. 1229-1239.

[28] Klinkrad, H. and Fritsche, B., “Assessment and Management of On-Ground Risk during Re-Entries”, Joint ESA-NASA Space-Flight Safety Conference, ESA SP-486, 2002. pp. 325-332.

[29] Lobachev, V., Pochukaev, V., Ivanov, N., et. al., “Navigation Support for the Salyut-7/Kosmos-1686 Orbiting Complex near Re-entry”, ESA Journal, Vol. 16, No. 2, 1992. pp. 209-216.

[30] Visentine, J.T., “Atomic Oxygen Effects Measurements for Shuttle Missions STS-8 and 41-G”, vols. I-III. NASA TM-100549, 1988.

[31] Mileti, S., Coluzzi, P., Marchetti, M., “Degradation of silicon carbide reflective surfaces in the LEO environment”, AIP Conference Proceedings, v 1087, p 67-74, 2009.

[32] Robinson, P.A., “Spacecraft Environmental Anomalies Handbook”, GL-TR-89-0222, Hanscom Air Force Base, MA: Air Force Geophysics Laboratory, 1989.

[33] Rodiek, J.A., Brandhorst, H.W., and O’Neill, M.J., “Stretched Lens Solar Array: The Best Choice for Harsh Orbits”, AIAA 2008-5755, 6th International Energy Conversion Engineering Conference, Cleveland, 28-30 July 2008.

[34] Weintraub, R. A., “Arth's Safe Zone Became Hot Zone During Legendary Solar Storms”, Goddard Space Flight Center, NASA.

[35] Ansell, J. I., Phillips, M. J., “Practical methods for reliability data analysis”, Oxford: Clarendon Press, 1994.

[36] Meeker, W. O., Escobar, L. A., “Statistical methods for reliability data”, New York: John Wiley & Sons, 1998.

[37] Rausand, M., Høyland, A., “System reliability theory: models, statistical methods, and applications”, 2nd ed. New Jersey: Wiley-Interscience, 2004.